CHARLES UNIVERSITY
Faculty of mathematics
and physics

Mathematical modeling of thermomechanical processes in terrestrial and planetary icy bodies

Ondřej Souček

Habilitation thesis

Mathematical Institute of Charles University

Field: Mathematics – Mathematical modeling and numerical mathematics

Prague 2022

To Klára & Míša

Contents

Preface

This thesis presents a summary of 11 manuscripts which I co-authored that have been published during the years 2011-2022 in international impacted peer-reviewed journals. They deal with mathematical modeling and numerical simulations of thermomechanical processes in terrestrial and planetary icy bodies, focusing, in particular, on the following three geophysical applications: *gravity-driven glacier flows*, *tidal deformation of planetary ice shells* of moons of giant planets, and *melting and meltwater transport* within these ice shells.

All the presented research involves development of tailored mathematical models and their numerical implementations through computer simulations when addressing specific applications. From this point of view, this work borders the disciplines of mathematical modeling and computational geophysics, which mirrors my academic and professional career (Ph.D. degree from Geophysics followed by a position as an Assistant Professor in the group of mathematical modeling).

Most of the presented research was done at my home institution, Faculty of Mathematics and Physics, Charles University, Prague, Czech Republic, but I benefited also from a one year stay at Dublin Institute for Advanced Studies, Ireland in 2010 and a seven months' stay at Laboratoire de Planétologie et Géosciences Nantes (LPGN), in France in 2012.

The presented research was done in collaboration with the following colleagues: Jaroslav Hron from the Mathematical Institute of Charles University, Marie Běhounková, Klára Kalousová and Ondřej Čadek from the Department of Geophysics, Faculty of Mathematics and Physics, Charles University, with French colleagues from LPGN Gabriel Tobie, Gaël Choblet, Olivier Bourgeois, Stéphane Pochat, and last but not least with my two current Ph.D. students Jiří Malík and Kateřina Pleiner Sládková, all of whom I would like to express my deepest gratitude for being my co-workers and friends. For great discussions and help I also thank Jan Blechta, Ladislav Hanyk, Martin Lanzendörfer, Michal Pavelka, Vít Průša, Sebastian Schwarzacher, Karel Tůma and Jakub Velímský. I would like to thank deeply also to my two mentors who have always been inspiring by their never-ending passion for science while remaining helping, encouraging and friendly - Professors Zdeněk Martinec and Josef Málek. I also thank to all my colleagues from the Mathematical Institute and from the Department of Geophysics at our Faculty of Mathematics and Physics for creating and maintaining a very friendly working environment.

The research presented in this thesis was supported by the following grants of the Czech Science Foundation 15-14263Y, 19-10809S, 22-20388S. I also acknowledge support from the Ministry of Education, Youth and Sports of the Czech Republic through the ERC-CZ project LL1202, the Czech Science Foundation project nr. 18-12719S, and computational resources of the IT4Innovations National Supercomputing Center, provided by the Ministry of Education, Youth and Sports from the Large Infrastructures for Research, Experimental Development and Innovations projects LM2015070 and LM2018140. Finally, I thank the University center for mathematical modeling, applied analysis and computational mathematics (UNCE MathMAC) for its support.

Introduction

This thesis is dedicated to mathematical modeling and computer simulations of physical processes in terrestrial and planetary icy bodies in the following geophysical applications:

- **Gravity-driven flows of glaciers** - formation and evolution of terrestrial and planetary grounded ice masses, which flow under the action of their own weight by a mechanism of *viscous creep* of the polycrystalline ice matrix over the time span of *years to hundreds of thousands of years*.
- **Tidal deformation of planetary ice shells** - periodic or quasi-periodic *elastic* or *viscoelastic deformation* of the ice shells of Europa and Enceladus, induced by the varying tidal potential raised by their primaries - Jupiter and Saturn - occurring on the time scale of *days*.
- **Melting and melt transport in planetary ice shells** by a reactive two-phase porous flow involving mechanical coupling between the deformation of the viscous ice matrix and the Darcy-type flow of the melt, which takes place on the time scale of *hundreds to millions of years* within the icy moons' shells.

Although the three types of physical processes listed above involve one and the same material - *water ice* - they differ significantly in its *material description* and also in the set of *simplifying assumptions* adopted in mathematical models of the processes. When describing glacier flow, ice is treated as a *non-Newtonian fluid* with stress and temperature-dependent viscosity. When deformed periodically by tides on a much shorter time scale of days, ice behaves more like an *elastic* or perhaps a *viscoelastic solid*. Finally, in the last of the three processes, when describing melting and melt transport, ice is often treated as a *porous two-phase medium*, i.e. a mixture of two components - liquid water and ice - which interact thermally and mechanically.

The general common framework used for the description and formulation of all the above processes is *continuum mechanics and thermodynamics*. Building blocks of continuum mechanics are mathematical abstractions of physical quantities as continuous and often smoothly differentiable fields. Relationships among these fields and their evolution are described by systems of partial differential equations (PDEs) equipped with suitable initial and boundary conditions. From a physical point of

view, these PDEs arise from generalizations of the traditional *conservation (or balance) laws* for mass, linear and angular momentum, energy, and entropy. Depending on the adopted detail of material description, one distinguishes between the *single* and *multi-component* variants of the continuum theory. In this thesis, the former framework suffices for capturing the first two models, while the latter - a two-component mixture model - is required to describe the third of the processes - melting and melt transport.

The structure of the thesis is the following. In the first chapter, I briefly review some of the physical properties of ice that enter the three discussed processes, with a particular emphasis on *ice rheology*. In the second chapter, I lay out the fundamentals of mathematical modeling of large-scale glacier flows and summarize the contents of two appended papers concerning this topic. Chapters three and four focus, in a similar manner, on the tidal deformation and on melting and melt transport, appending 5 and 4 research papers, respectively. In the last chapter, I provide an outlook of my short and mid-term future research plans and ideas in the direction of the three respective topics.

Water ice rheology 1

Water ice has been detected or indirectly inferred on most planets and moons in the Solar System making it one of the most ubiquitous known volatile materials. Currently, more than seventeen different crystalline structures of water ice are known (Salzmann, 2019) plus several other amorphous ones. However, terrestrial cryosphere, i.e. the solid water part of the Earth's climate system, as well as the outermost layers of so-called icy moons in the Solar System, addressed in this thesis, are composed of the low-pressure ice phase **$\mathbf{I}_h$ - hexagonal ice**.

An ice I_h monocrystal is composed of water molecules arranged in a (bi)planar hexagonal pattern as in Figure 1.1 (left). The layer with hexagonal rings constitutes so-called *basal plane* and the axis perpendicular to it is the *optical* or *c-axis*. Due to this arrangement, an ice I_h crystal exhibits hexagonal symmetry with respect to the basal plane and, due to relatively weak bond between the neighboring basal planes, also a strong mechanical anisotropy.

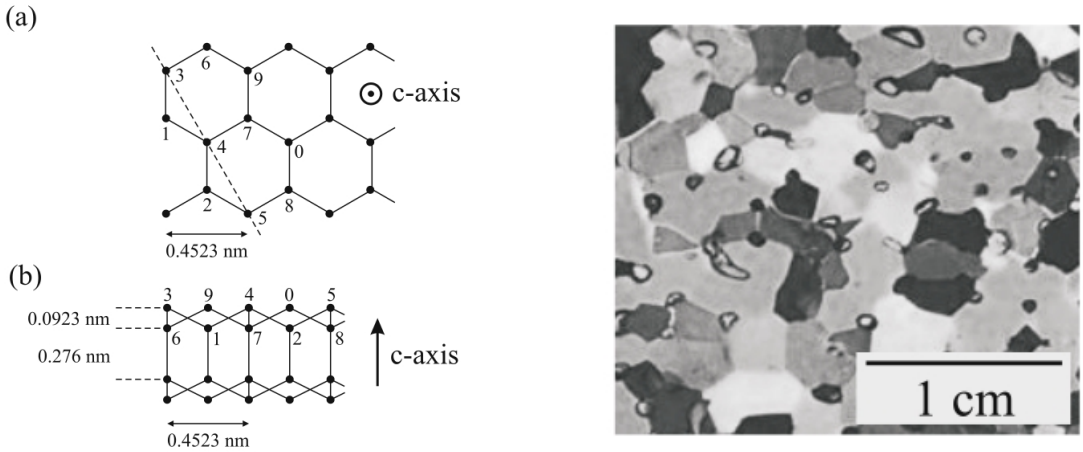

Figure 1.1: A diagram of molecular structure of hexagonal ice I_h monocrystal (left) and a photograph of polycrystalline glacier ice between polarisation filters (right). Both taken from Greve and Blatter (2009).

In nature, however, ice occurs primarily as a *polycrystalline* material, i.e. an aggregate of individual ice grains, see Figure 1.1 (right). Unless arranged by flow or specific growth conditions, the orientation of the grains is random, so the resulting

material behaves as isotropic despite the strong anisotropy of the individual ice grains.

Even though isotropic, mechanical behavior of polycrystalline ice is still rather complex. The monocrystals themselves exhibit a wide range of deformation regimes from elastic and viscoelastic to viscous and plastic, and when combined in a polycrystalline structure, additional deformation mechanisms associated with the processes at grain boundaries or recrystallization add to the complexity. The characteristic creep response of polycrystalline ice I_h specimen in a simple shear experiment is sketched in Figure 1.2.

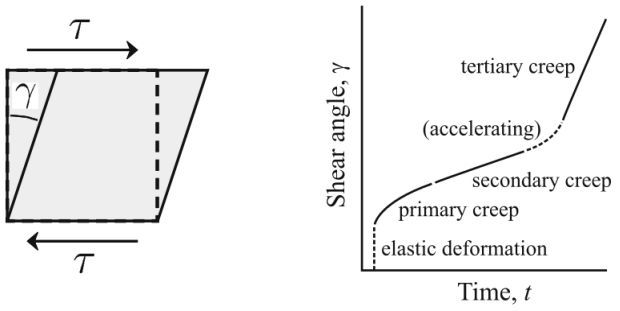

Figure 1.2: Characteristic creep curve of polycrystalline ice (right) in a simple shear experiment (left), taken from Greve and Blatter (2009).

After an immediate *elastic response* to the loading, the deformation passes through several stages. *Primary creep* is a phase with decreasing rate of deformation attributed to a gradually increasing amount of geometric incompatibilities in the polycrystalline aggregate with different crystal orientations. After reaching the minimum shear rate, the next phase is called a *secondary creep* which is stationary unless thermal or stress state of the material allows for so-called *dynamic recrystallization*, i.e. structural changes in the polycrystalline material that provide a larger amount of crystals with orientation favorable to deformation. If this process initiates, the deformation rate further increases until reaching a new steady state with larger deformation rate compared to the secondary creep - a phase of *tertiary creep.*

Let us briefly summarize some of these mechanical properties and describe the basics of ice rheology.

1.1 Elastic properties of ice

The mechanical response of ice I_h is elastic in the regime of small strains and high frequencies. Under these assumptions, ice can be described as an anisotropic Hookean

(elastic) solid in terms of a 4-th order tensor of elastic parameters $\mathcal{C}$, which relates the components of small strain tensor $\boldsymbol{\varepsilon} = \frac{1}{2}(\nabla\mathbf{u} + (\nabla\mathbf{u})^T)$ ($\mathbf{u}$ denoting the displacement), and the Cauchy stress $\boldsymbol{\sigma}$ by (using Einstein's summation convention):

$$\boldsymbol{\sigma}_{ij} = \mathcal{C}_{ijkl}\boldsymbol{\varepsilon}_{kl}\,. \tag{1.1a}$$

Out of the 21 independent coefficients for a general anisotropic solid, only 5 are independent for the ice I_h monocrystal due to its hexagonal symmetry. The tensor of elastic parameters is then usually written in the Voigt 6×6 representation as

$$\widetilde{\boldsymbol{\sigma}}_\alpha = \widetilde{\mathcal{C}}_{\alpha\beta}\widetilde{\boldsymbol{\varepsilon}}_\beta\,, \qquad \alpha,\beta = 1,\ldots,6\,, \tag{1.1b}$$

where

$$(\widetilde{\boldsymbol{\sigma}}_1,\widetilde{\boldsymbol{\sigma}}_2,\widetilde{\boldsymbol{\sigma}}_3,\widetilde{\boldsymbol{\sigma}}_4,\widetilde{\boldsymbol{\sigma}}_5,\widetilde{\boldsymbol{\sigma}}_6) = (\boldsymbol{\sigma}_{11},\boldsymbol{\sigma}_{22},\boldsymbol{\sigma}_{33},\boldsymbol{\sigma}_{23},\boldsymbol{\sigma}_{13},\boldsymbol{\sigma}_{12})\,, \tag{1.1c}$$

$$(\widetilde{\boldsymbol{\varepsilon}}_1,\widetilde{\boldsymbol{\varepsilon}}_2,\widetilde{\boldsymbol{\varepsilon}}_3,\widetilde{\boldsymbol{\varepsilon}}_4,\widetilde{\boldsymbol{\varepsilon}}_5,\widetilde{\boldsymbol{\varepsilon}}_6) = (\boldsymbol{\varepsilon}_{11},\boldsymbol{\varepsilon}_{22},\boldsymbol{\varepsilon}_{33},\boldsymbol{\varepsilon}_{23},\boldsymbol{\varepsilon}_{13},\boldsymbol{\varepsilon}_{12})\,, \tag{1.1d}$$

and it holds (Schulson and Duval, 2009):

$$\widetilde{\mathcal{C}} = \begin{pmatrix} \mathcal{C}_{11} & \mathcal{C}_{12} & \mathcal{C}_{13} & 0 & 0 & 0 \\ \mathcal{C}_{12} & \mathcal{C}_{11} & \mathcal{C}_{13} & 0 & 0 & 0 \\ \mathcal{C}_{13} & \mathcal{C}_{13} & \mathcal{C}_{33} & 0 & 0 & 0 \\ 0 & 0 & 0 & \mathcal{C}_{44} & 0 & 0 \\ 0 & 0 & 0 & 0 & \mathcal{C}_{44} & 0 \\ 0 & 0 & 0 & 0 & 0 & \frac{\mathcal{C}_{11}-\mathcal{C}_{12}}{2} \end{pmatrix}. \tag{1.1e}$$

Elastic response of polycrystalline aggregates of randomly oriented ice I_h monocrystals is isotropic despite their individual anisotropy, as the response gets averaged out. Consequently, only two elastic Lamé parameters characterize the elastic properties of polycrystalline ice, for instance the *shear modulus* μ and the *second Lamé parameter* λ, and it holds

$$\boldsymbol{\sigma} = (\lambda\mathrm{Tr}\boldsymbol{\varepsilon})\,\mathbb{I} + 2\mu\boldsymbol{\varepsilon}\,, \tag{1.2a}$$

or, alternatively, using *Young's modulus* E and the *Poisson ratio* ν

$$\boldsymbol{\sigma} = \frac{E\nu}{(1+\nu)(1-2\nu)}\mathrm{Tr}\boldsymbol{\varepsilon}\,\mathbb{I} + \frac{E}{(1+\nu)}\boldsymbol{\varepsilon}\,. \tag{1.2b}$$

The two pairs of parameters are related by

$$E = \frac{\mu(3\lambda+2\mu)}{\lambda+\mu}\,, \qquad \nu = \frac{\lambda}{2(\lambda+\mu)}\,, \tag{1.2c}$$

$$\lambda = \frac{E\nu}{(1+\nu)(1-2\nu)}\,, \qquad \mu = \frac{E}{2(1+\nu)}\,. \tag{1.2d}$$

Parameter	Value	Unit
Youngs' modulus E	$9.33\times\ 10^9$	Pa
Poisson's ratio ν	0.325	-
Lamé parameter λ	6.54×10^9	Pa
Shear modulus μ	3.52×10^9	Pa

Table 1.1: Elastic moduli for isotropic polycrystalline ice at $\vartheta = -16°\mathrm{C}$.

Characteristic values of these parameters, taken from Petrenko and Whitworth (2002) (at $\vartheta = -16°\mathrm{C}$), are shown in Table 1.1.

The experimentally measured temperature dependence of the elastic parameters of ice is relatively mild and can be approximated by (Petrenko and Whitworth, 2002)

$$X(\vartheta) = X_0(1 - 1.42 \times 10^{-3}(\vartheta[°\mathrm{C}] + 16))\,, \tag{1.3}$$

where X stands for E, λ, μ and X_0 for their reference values at $\vartheta = -16°\mathrm{C}$; Poisson ratio ν does not change with temperature significantly.

1.2 Ductile creep of ice

When subjected to mechanical forcing by shear stress, ice deforms by a combination of creep processes and would continue to do so indefinitely – in this regard, on the long time scales, polycrystalline ice behaves as a viscous fluid, contrary to our everyday experience with it as a crystalline solid. A number of mechanisms govern and determine the creep response of ice both at the level of single ice grains or the polycrystalline aggregate.

1.2.1 Plastic deformation of ice monocrystals

As the individual basal planes of ice I_h monocrystals are relatively distant apart compared to the distances of molecules and atoms in the basal crystal plane (see Figure 1.1b)), when the crystal is subjected to a mechanical shear stress with respect to the basal plane, the neighboring basal planes tend to glide with respect to each other. As the bond between the individual basal planes is by far the weakest one in the crystalline structure, this makes the process of *basal slip* a dominant deformation mechanism for the ice I_h monocrystal. While possible, deformation in other than basal planes is much more difficult, so the creep response of I_h monocrystals is generally anisotropic. Deformation of a single ice crystal is also possible through creation and motion of dislocations - imperfections in the crystalline structure, which

allow for deformation even for relatively small applied stresses by the process of *dislocation creep*. For practical purposes, it is more important, however, to study the creep response of polycrystalline ice.

1.2.2 Creep of polycrystalline ice

High-stress regime - Glen's flow law

In terrestrial glaciers, ice deforms primarily by the secondary creep and the stress-strain-rate relation most commonly used in modeling is the so-called *Glen's flow law* (Glen, 1952), relating the traceless part $\mathbb{S}$ of the total Cauchy stress tensor $\boldsymbol{\sigma}$ to the symmetric part of the velocity gradient $\mathbb{D}(\mathbf{v})$ (also traceless due to assumed ice incompressibility). It reads

$$\boldsymbol{\sigma} = -p\mathbb{I} + \mathbb{S}\,, \qquad \mathbb{D}(\mathbf{v}) = \frac{1}{2\eta}\mathbb{S}\,, \qquad \text{with} \qquad \frac{1}{2\eta} = \mathcal{A}(p,\vartheta)\mathbb{S}_{II}^{n-1}\,, \tag{1.4}$$

where p denotes the pressure (mean normal stress), η is the ice viscosity, $\mathcal{A}$ is a rate factor depending on pressure and temperature ϑ and $\mathbb{S}_{II}$ denotes the second invariant of $\mathbb{S}$, given (since $\mathbb{S}$ is traceless) by

$$\mathbb{S}_{II} = \sqrt{\frac{\mathbb{S} : \mathbb{S}}{2}} = \sqrt{\frac{\mathbb{S}_{ij}\mathbb{S}_{ij}}{2}}\,. \tag{1.5}$$

Based on laboratory experiments, the exponent n=3 is traditionally considered for terrestrial glaciers – this constitutes the Glen's flow law (Glen, 1952). Recently, (uniaxial loading) experiments at differential stresses exceeding 1 MPa (i.e. in the high-stress regime) indicated higher exponents up to n=4 associated with the regime of *dislocation creep*, while for slightly lower stresses, transition to a lower exponent n=1.8 and n=2.4 has been observed and attributed to a mechanism of *grain-boundary sliding (GBS)-limited creep* and *basal slip (BS)-limited creep*, respectively (Durham et al., 2010). From this point of view, Glen's flow law represents certain averaged-out flow law over this range of stress regimes.

Relation (1.4) can be inverted, which yields

$$\mathbb{S} = 2\eta\mathbb{D}(\mathbf{v})\,, \qquad \text{with} \qquad \eta = \frac{1}{2}\mathcal{A}(\vartheta,p)^{-\frac{1}{n}}\mathbb{D}_{II}^{\frac{1-n}{n}}\,, \tag{1.6}$$

where $\mathbb{D}_{II}$ is the second invariant of $\mathbb{D}(\mathbf{v})$. Note that given n=3 for Glen's flow law, ice behaves in this regime as a *shear thinning material* - its viscosity η decreases with the increasing rate of deformation. The rate factor $\mathcal{A}$ in Glen's flow law is of Arrhenius type (e.g. Greve and Blatter, 2009):

$$\mathcal{A}(\vartheta,p) = \mathcal{A}_0\, e^{-(E+pV)/R\vartheta}\,, \tag{1.7}$$

where E is the activation energy, V is the activation volume, R the universal gas constant and $\mathcal{A}_0$ is a parameter. The dependence of rate factor $\mathcal{A}$ on the confining pressure p is basically limited to pressure dependence of the melting point Greve and Blatter (2009). By introducing temperature relative to the melting point $\vartheta' = \vartheta - \vartheta_m(p) + \vartheta_0$, with ϑ_0=273.15 K and with the melting point $\vartheta_m(p)$ given by Clausius-Clapeyron relation $\vartheta_m(p) = \vartheta_0 - \beta p$, where β=7.42×10^{-8}K Pa^{-1} and 9.8×10^{-8} K Pa^{-1} for pure and air-saturated ice, respectively (Hooke, 2005), the rate factor can be simplified as follows

$$\mathcal{A}(\vartheta') = \tilde{\mathcal{A}}_0 \, e^{-\tilde{E}/R\vartheta'} \, . \tag{1.8}$$

Low-stress regime

For differential stresses below 0.1−0.2 MPa which are relevant for the ductile parts of planetary ice shells (Durham et al., 2001), but probably also for large polar ice sheets on Earth, the simple Glen's flow law with n=3 most likely no longer holds, as indicated by experimental studies (e.g. Dahl-Jensen and Gundestrup, 1987; Goldsby and Kohlstedt, 2001).

Dislocation accommodated grain boundary sliding becomes the dominant deformation mechanism replacing the dislocation creep. Consequently there is a transition to an exponent of n=1.8 (*GBS-limited creep*) and at even lower stresses n=2.4 (*BS-limited creep*). Furthermore, Newtonian behavior, i.e n=1, has been theoretically predicted for stresses as low as 75 kPa and attributed to the process of *diffusion accommodated grain boundary sliding* or *diffusion creep* (Durham et al., 2001).

A diagram of various deformation mechanisms based on the stress regime, and their comparison with Glen's flow law are shown in Figure 1.3.

Composite creep

The four deformation mechanisms of polycrystalline ice I$_h$ - dislocation creep, grain boundary sliding, basal slip and diffusion creep are all characterized by a general viscosity dependence of the form

$$\eta_i = \frac{1}{2} \frac{d^{m_i}}{A_i \, \mathbb{S}_{II}^{n_i - 1}} \exp\left(\frac{E_i + pV_i}{R\vartheta}\right) , \tag{1.9}$$

where, compared to Glen's flow law, an explicit dependence on the grain size d is considered and the remaining parameters are analogous to Glen's flow law, but the exponents, activation energies and volumes differ for the individual mechanisms. The values of these parameters based on Goldsby and Kohlstedt (2001) are listed in Table 1.2.

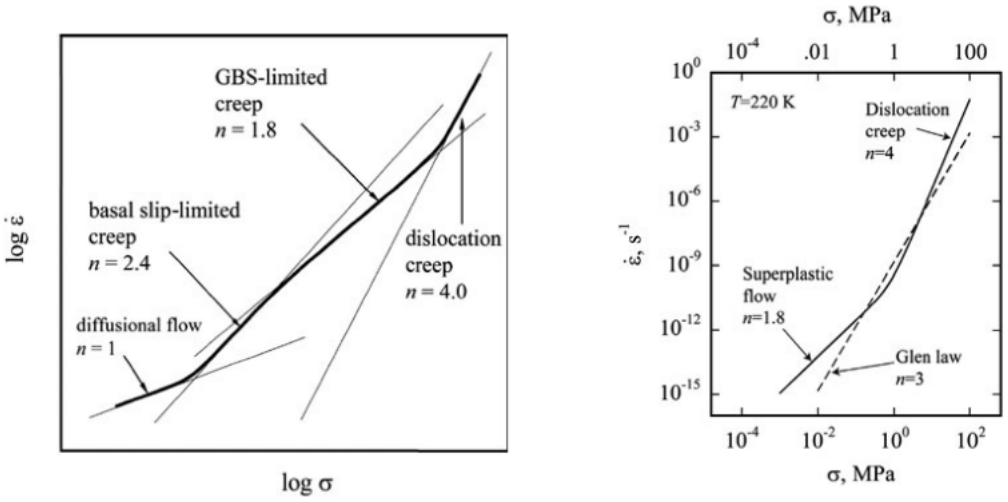

Figure 1.3: Left: a diagram of creep regimes for ice I_h, taken from Goldsby and Kohlstedt (2001). Right: comparison of Glen's flow law and dislocation creep/superplastic flow, taken from Durham et al. (2010).

Mechanism	A ($\mathrm{Pa}^{-n} \cdot \mathrm{m}^m \cdot \mathrm{s}^{-1}$)	n	m	E ($\mathrm{kJ} \cdot \mathrm{mol}^{-1}$)
Dislocation ($\vartheta \leq 258$ K)	$4.0 \cdot 10^{-19}$	4.0	0.0	60
Dislocation ($\vartheta > 258$ K)	$6.0 \cdot 10^{4}$	4.0	0.0	180
GBS ($\vartheta \leq 255$ K)	$6.2 \cdot 10^{-14}$	1.8	1.4	49
GBS ($\vartheta > 255$ K)	$5.6 \cdot 10^{15}$	1.8	1.4	192
BS	$2.2 \cdot 10^{-7}$	2.4	0.0	60
Diffusion	$3.3 \cdot 10^{-10}$	1.0	2.0	59

Table 1.2: Values of creep mechanism parameters, based on Goldsby and Kohlstedt (2001), activation volume for all mechanisms usually considered to be $V = -13 \times 10^{-6}$ m^3 mol^{-1}.

A semi-empirical composite creep flow law combining all of the above mechanisms has been suggested by Goldsby and Kohlstedt (2001) and formulated in terms of an *effective viscosity* η_{eff} of the form

$$\frac{1}{\eta_{\mathrm{eff}}} = \frac{1}{\eta_{\mathrm{diff}}} + \frac{1}{\eta_{\mathrm{disl}}} + \frac{1}{\eta_{\mathrm{bs}} + \eta_{\mathrm{gbs}}} \,. \tag{1.10}$$

In applications, this expression is sometimes augmented by a term $\frac{1}{\eta_{\max}}$ which limits the viscosity from above by $\eta_{\max}$. In planetary applications, this is necessary to prevent the models from predicting unrealistically high stresses in the upper very

cold parts of the ice shells where the standard temperature-viscosity relations predict extreme viscosity values. In these regions, the active stress release mechanism is probably *brittle failure* or *plastic deformation* rather than viscous creep, which are not considered in the above model.

A practical simplification of the non-linear composite rheology is sometimes possible by assuming locally certain fixed stress and grain-size regime while keeping general temperature dependence. Absorbing the rest of the complexities into a reference viscosity η^0_{eff} at some reference temperature ϑ_{ref}, yields the following viscosity formula

$$\eta_{\text{eff}} = \eta^0_{\text{eff}} \exp\left(\frac{E_i}{R}\left(\frac{1}{\vartheta} - \frac{1}{\vartheta_{\text{ref}}}\right)\right). \tag{1.11}$$

1.2.3 Effect of grain size

Noting that both grain boundary sliding and diffusion creep depend strongly on the grain size (representing so-called *grain size sensitive creep*), the actual state and evolution of this ice property is both very important, but unfortunately also largely unconstrained in most applications. In terrestrial glaciers, the grain size varies typically between 1 and 10 mm, but much larger grain sizes have been predicted on Europa (up to 80 mm), unless tidal flexing contributes to recrystallization, in which case the maximum grain size would be $\sim$ 1 mm (Barr and McKinnon, 2007).

From the physical point of view, grain size evolution is determined by a dynamic equilibrium between two competing processes - spontaneous grain growth and dynamic grain size reduction by recrystallization. The first process is thermodynamically driven by reducing the interfacial free energy, the other is related with the free energy of dislocations (e.g. Schulson and Duval, 2009; Barr and McKinnon, 2007). The equilibrium grain size depends on the stress and can be approximated as (Barr and McKinnon, 2007)

$$\frac{d}{b} = D\left(\frac{\sigma}{\mu}\right)^{-1.25}, \tag{1.12}$$

where b is the Burger's vector for ice, D is a dimensionless parameter (of the order 10-100), σ is stress amplitude, and μ is the shear modulus. The above holds for pure water ice. If additional impurities are present, such as dust or clathrates, pinning of ice grain boundaries at these impurities further reduces the maximum grain size (Durand et al., 2006).

1.2.4 Effect of melt

Partial melting within the ice matrix enhances its ductile deformation. Since melt is first produced at grain boundaries, the effect of liquid phase is primarily associated

with promotion of grain boundary sliding (Schulson and Duval, 2009). When the melting point is approached, certain weakening and the so-called *pre-melting effects* are manifested in the form of a change of the corresponding activation energies and of the rate prefactors for both the grain boundary sliding and also the dislocation creep (see Table 1.2). Melt presence characterized by a volume fraction ϕ leads to a strong reduction of the effective viscosity (De La Chapelle et al., 1999), which may be parameterized by (Tobie et al., 2003)

$$\eta_{\text{eff}} = \eta^0_{\text{eff}} \exp\left(-\gamma\phi\right), \tag{1.13}$$

with γ=45 in order to provide the observed reduction of viscosity by an order of magnitude for a 5% porosity increase.

1.2.5 Ductile-to-brittle transition

At high-enough differential stresses (and often low-enough temperatures), for instance in the near-surface regions of tidally loaded icy moons or at the surfaces of glaciers flowing sufficiently fast over undulated bedrock topography, the ductile creep becomes inefficient in its capacity of accommodating stress within the ice and another deformation mechanism gets triggered - brittle failure, i.e. creation and propagation of cracks. Linear elastic fracture mechanics (LEFM) provides energy-based criteria for cracks initiation and propagation depending on various regimes of mechanical loading (see e.g. van der Veen, 1998; Schulson and Duval, 2009).

While we shall not pursue this topic here, let us only mention that in planetary applications, for instance in Europa's ice shell, a *brittle-to-ductile transition*, separating the top brittle and bottom ductile parts, is expected to occur at a depth characterized by conditions at which the stresses associated with ductile creep become comparable with the fracture toughness of ice at the given temperature (e.g. Nimmo and Manga, 2009).

1.3 Viscoelastic properties of polycrystalline ice

When subjected to periodic mechanical loading on the time scale of hours and days, for instance by tides on icy moons raised on them by their primaries, ice is neither viscous nor perfectly elastic, but rather viscoelastic. This anelasticity of ice in the process of tidal deformation results in dissipation of mechanical energy, which may play a significant or even principal role in the energy budget of the moons. Through mechanical dissipation, the tidal deformation thus greatly contributes to the icy moons' internal evolution and may be critical in providing the energy supply for

creating and maintaining internal oceans (e.g. Tobie et al., 2005; Roberts, 2015; Beuthe, 2016; Choblet et al., 2017).

Aneleaticity of ice subjected to periodic tidal loading is a consequence of microstructural changes in the material. This implies that the deformation is not fully recoverable upon unloading, but contains an irreversible component. There is an experimental evidence that the mechanisms of the irreversible deformation include those that have been described in the previous section on ductile viscous creep, such as the dislocation creep or grain boundary sliding (McCarthy and Castillo-Rogez, 2013; Webb and Jackson, 2003). This then justifies the use of the same notion of viscosity in the two very different processes - viscous creep on geological time scale and periodic tidal deformation on the time scale of days. However, some caution is necessary since the strains induced by tides are very small compared to those resulting from viscous creep on geological time scales, so the regimes at which these mechanisms operate differ significantly.

In planetary applications considered here, the viscoelastic response of ice is usually limited to the shear component of the deformation, while the bulk component is elastic. Due to the small strain deformation regime, linear models of viscoelasticity are mostly considered and the complexities of nonlinear viscosity are suppressed or parameterized. For linear models, viscoelasticity can be characterized in terms of compliance J relating the deviatoric part of the Cauchy stress $\mathbb{S}$ and the deviatoric part of the strain tensor $\boldsymbol{\varepsilon}^d$ (Efroimsky, 2012):

$$2\boldsymbol{\varepsilon}^d = \int_{-\infty}^{t} J(t-\tau)\dot{\mathbb{S}}(\tau,\cdot)d\tau\,, \tag{1.14}$$

or in the frequency domain:

$$2\widehat{\boldsymbol{\varepsilon}^d}(\omega) = \bar{J}(\omega)\widehat{\mathbb{S}}(\omega)\,, \qquad \text{where} \qquad \bar{J}(\omega)= \int_0^{\infty} \dot{J}(\tau)e^{-i\omega\tau}\,d\tau\,, \tag{1.15}$$

and the Fourier images of $\boldsymbol{\varepsilon}^d$ and $\mathbb{S}$ are denoted by $\widehat{\boldsymbol{\varepsilon}^d}$, and $\widehat{\mathbb{S}}$, respectively.

A number of various viscoelastic models have been proposed, see McCarthy and Castillo-Rogez (2013) for a review. Those most commonly used in applications discussed here, i.e. for the investigation of tidal dissipation in planetary ice shells, are the *Maxwell* and the *Andrade models*, with the compliances given by

$$J(t-\tau) = \begin{cases} \frac{1}{\mu}\left(1+\frac{t-\tau}{\tau_M}\right)H(t-\tau) & \text{Maxwell} \\ \frac{1}{\mu}\left(1+\frac{t-\tau}{\tau_M}+\left(\frac{t-\tau}{\zeta_A\tau_M}\right)^{\alpha}\right)H(t-\tau) & \text{Andrade} \end{cases} \tag{1.16}$$

or in the frequency domain

$$\bar{J}(\omega) = \begin{cases} \frac{1}{\mu}\left(1-\frac{i}{\omega\tau_M}\right) & \text{Maxwell} \\ \frac{1}{\mu}\left(1-\frac{i}{\omega\tau_M}+(i\omega\zeta_A\tau_M)^{-\alpha}\Gamma(1+\alpha)\right) & \text{Andrade} \end{cases}\,. \tag{1.17}$$

Here τ_M denotes the Maxwell time defined by $\tau_M = \frac{\eta}{\mu}$ with η being viscosity, ζ_A and α are parameters, H is the Heaviside function and Γ denotes the Gamma function.

Maxwell model is popular due to its extreme simplicity both in terms of implementation and also regarding the frequency-characterization of mechanical dissipation - it has a single global maximum for the frequency $\omega = \frac{1}{\tau_M}$. Maxwell model thus predicts heating maximum when the forcing (tidal) period equals the Maxwell time.

Considering temperature-dependence of viscosity (e.g. as in (1.11)), allows one to look for a coupled evolution of tidal response and internal dynamics of the bodies (e.g. Tobie et al., 2005, 2008; Běhounková et al., 2012; Souček et al., 2019). A deficiency of the Maxwell model is that is seems to underestimate the dissipation for smaller forcing periods than the Maxwell time. A more accurate parameterization is provided by the Andrade model (Castillo-Rogez et al., 2011; Běhounková et al., 2015) or its Maxwell-type approximation (Běhounková et al., 2013; Souček et al., 2019).

Gravity-driven glacier flow 2

This chapter aims to briefly introduce the framework for mathematical modeling of *gravity-driven flows of glaciers and ice sheets*, introduce the traditional *shallow ice approximation* and point out its advantages and shortcomings. This is followed by a summary of the results of two appended papers that concern numerical modeling of glacial processes.

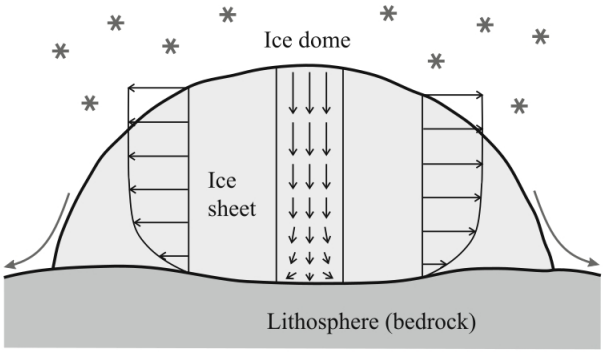

Figure 2.1: A sketch of an ice sheet, from Greve and Blatter (2009).

The fundamental processes that govern the evolution and dynamics of terrestrial and planetary ice sheets and glaciers are relatively simple. Local climatic and atmospheric conditions - primarily the spatio-temporal temperature and precipitation patterns - lead, in favorable areas and periods, to annual deposition of snow and ice that exceed the annual melting and sublimation. This results in gradual snow deposition, compaction by its own weight and subsequent snow-ice transformation and ice mass build-up, i.e. formation of a glacier. If these favorable conditions persist for sufficiently long time, the glacier volume increases. The shear stresses gradually building up within the ice matrix eventually trigger internal creep and the glacier starts deforming and flowing downstream unless hindered by bedrock topography, see an illustrative sketch in Figure 2.1.

2.1 Mathematical model of glacier flow

For the description of flows of glaciers and ice sheets on Earth (and possibly other planets like Mars in its ancient past), ice is usually treated as a *non-Newtonian viscous fluid* with viscosity depending on the stress/strain rate, pressure and temperature. The mathematical model describing glacier evolution is formulated in terms of the balance equations of continuum mechanics - *balances of mass, linear and angular momentum and internal energy.* The scaling arguments based on the identification of characteristic scales of all the involved physical quantities and the associated dimensionless formulation of the balance equations, allow one to reduce the general model and arrive at a simpler approximate one. In the given application, the traditionally adopted assumptions involve *incompressibility* of the material and negligible inertial forces (in the sense of negligible Froude number). Consequently, the resulting system comprising the balances of mass, linear momentum and energy takes the following form of three partial differential equations for ice velocity $\mathbf{v}$, pressure p and (absolute) temperature ϑ (Greve and Blatter, 2009):

$$\operatorname{div}\mathbf{v} = 0\,, \tag{2.1a}$$

$$\mathbf{0} = -\nabla p + \operatorname{div}\mathbb{S} + \rho_i\mathbf{g}\,, \tag{2.1b}$$

$$\rho_i C_v(\vartheta)\left(\frac{\partial\vartheta}{\partial t} + \mathbf{v}\cdot\nabla\vartheta\right) = \operatorname{div}\left(k(\vartheta)\nabla\vartheta\right) + \mathbb{S}:\mathbb{D}(\mathbf{v})\,. \tag{2.1c}$$

Here $\mathbf{g}$ is the gravity acceleration, ρ_i the ice density, and C_v and k are the heat capacity and the thermal conductivity of ice, respectively. Mechanical response (rheology) of ice is described by specifying the dependence of the (symmetric) deviatoric stress tensor $\mathbb{S}$ on p, ϑ and the symmetric part of the velocity gradient $\mathbb{D}(\mathbf{v}) = \frac{1}{2}(\nabla\mathbf{v} + \nabla^T\mathbf{v})$. As discussed in the previous chapter, for terrestrial glaciers, the viscous creep regime is usually considered in the high-stress limit, corresponding to dislocation creep or its transition to superplastic flow. It is parameterized in terms of an empirical relationship known as *Glen's flow law* (Glen, 1952; Glen and Perutz, 1955) describing ice as a non-Newtonian power-law fluid by specifying

$$\mathbb{D}(\mathbf{v}) = \mathcal{A}(\vartheta,p)\mathbb{S}_{II}^{n-1}\mathbb{S}\,. \tag{2.2a}$$

Written in a more standard (inverse) form using viscosity η, it reads

$$\mathbb{S} = 2\eta\mathbb{D}(\mathbf{v})\,, \qquad \text{with} \qquad \eta = \frac{1}{2}\mathcal{A}(\vartheta,p)^{-\frac{1}{n}}\mathbb{D}_{II}^{\frac{1-n}{n}}\,. \tag{2.2b}$$

Here $\mathbb{S}_{II}$ and $\mathbb{D}_{II}$ denote the (scalar) second invariants of the two tensors, the power-law exponent for Glen's flow law is n=3 and the rate factor $\mathcal{A}(\vartheta,p)$ is given by (1.7) or (1.8). The heat capacity of ice depends on temperature linearly in the range of

terrestrial temperatures and the dependence is moderate and given by (Ritz, 1987)

$$C_v(\vartheta) = (146.3 + 7.253\vartheta[\mathrm{K}])\mathrm{Jkg}^{-1}\mathrm{K}^{-1}\,. \tag{2.3a}$$

The temperature dependence of the thermal conductivity reads (Ritz, 1987)

$$k(\vartheta) = 9.828e^{-0.0057\vartheta[\mathrm{K}]}\mathrm{Wm}^{-1}\mathrm{K}^{-1}\,. \tag{2.3b}$$

The governing equations, obtained by inserting the rheology (2.2) and the material parameters (2.3) into the balance equations (2.1), need to be accompanied by the boundary conditions at all interfaces of the glacier with its surroundings. These can be in a very general way formulated as expressions of the form

$$g_i(\vartheta, p, \mathbf{q}\cdot\boldsymbol{n}, \mathbf{v}_n, \mathbf{v}_\tau, \mathbb{S}\boldsymbol{n}) = 0\,, \qquad i = 1, 2...\,, \tag{2.4a}$$

describing relationships among state variables ϑ, p, normal and tangential velocity components $\mathbf{v}_n$, $\mathbf{v}_\tau$, normal component of the heat flux $\mathbf{q} = -k\nabla\vartheta$ and the traction force $\mathbb{S}\boldsymbol{n}$ ($\boldsymbol{n}$ denoting the outer surface unit normal). A particular example of such set of boundary conditions for a cold (i.e. non-temperate) grounded glacier with two distinct interfaces - upper free surface and bottom ice-bedrock interface - would be as follows.

- Upper glacier surface:

$$(-p\mathbb{I} + \mathbb{S})\boldsymbol{n} = -p^{\mathrm{atm}}\boldsymbol{n}\,, \qquad \vartheta = \vartheta^s\,, \tag{2.4b}$$

  specifying mechanically free surface (exposed to atmospheric pressure p^{atm}) and surface temperature ϑ^s (depending explicitly on position and time).

- Ice-bedrock interface:

$$\mathbf{q}\cdot\boldsymbol{n} = \begin{cases} -q^{\mathrm{geo}} & \text{if} \quad \vartheta < \vartheta^{\mathrm{melting}} \\ -q^{\mathrm{geo}} + \mathbf{v}\cdot\mathbb{S}\boldsymbol{n} + La^b & \text{if} \quad \vartheta = \vartheta^{\mathrm{melting}} \end{cases}\,, \tag{2.4c}$$

  and

$$\mathbf{v}_n = \begin{cases} 0 \\ \boldsymbol{\nu}_n + a^b/\rho_i\,, \end{cases}\,, \qquad \mathbf{v}_\tau = \begin{cases} \mathbf{0} & \text{if} \quad \vartheta < \vartheta^{\mathrm{melting}} \\ -\alpha(\mathbb{S}\boldsymbol{n})_\tau & \text{if} \quad \vartheta = \vartheta^{\mathrm{melting}} \end{cases}\,. \tag{2.4d}$$

  Both the thermal and the mechanical basal conditions distinguish between the "frozen" base regime ($\vartheta < \vartheta^{\mathrm{melting}}$) and the "temperate" base regime ($\vartheta = \vartheta^{\mathrm{melting}}$) in which melting/freezing may take place.

  The first condition (2.4c) specifies either continuity of the normal heat flux with the geothermal heat flux q^{geo} or relates the melting/freezing rate a^b (positive for melting) at the bottom interface (L denoting the latent heat of melting) with the jump of the heat fluxes and frictional heating power at the glacier base (term $-\mathbf{v}\cdot\mathbb{S}\boldsymbol{n}$).

The second condition (2.4d) determines the normal and tangential components of the ice velocity at the glacier base. The normal component is zero for frozen bed conditions, or, is given by the melting rate a^b and the normal component of the bedrock velocity vector $\boldsymbol{\nu}_n$ at a temperate base. The latter is an independent quantity that can be obtained, for instance by coupling the glacier model with a model of deformation of the underlying medium (Earth's lithosphere) in a process of so-called glacial isostatic adjustment (see e.g. Tarasov and Peltier (2002); Tarasov et al. (2012)). The tangential part of (2.4d) is a stick/slip sliding law in glacilogy often considered to be of Weertman type (Weertman (1957), Boulton and Hindmarsh (1987)), in which case the sliding coefficient α is of the form

$$\alpha = \alpha_0 \frac{|(\boldsymbol{\sigma n})_\tau|^p}{|(\boldsymbol{\sigma n})_n|^q}\,, \tag{2.4e}$$

i.e. depending on p, q, powers of the tangent and normal tractions $(\boldsymbol{\sigma n})_\tau = \boldsymbol{\sigma n} - (\boldsymbol{n}\cdot\boldsymbol{\sigma n})\boldsymbol{n}$, $(\boldsymbol{\sigma n})_n = \boldsymbol{n}\cdot\boldsymbol{\sigma n}$.

After providing the initial conditions in terms of initial temperature distribution and initial geometry of the glacier, the problem of glacier thermo-mechanical evolution comprises the solution of the above system of governing equations alongside with the *kinematic condition*, i.e. *evolution equation for ice geometry*. If the ice geometry is described by an elevation function f^s (describing the elevation of the glacier surface over some fixed reference plane surface), the kinematic condition (in global Cartesian coordinate system) reads

$$\frac{\partial f^s}{\partial t} + \mathbf{v}_x \frac{\partial f^s}{\partial x} + \mathbf{v}_y \frac{\partial f^s}{\partial y} - \mathbf{v}_z = a^s(t,x,y,z)\,. \tag{2.5}$$

The source term a^s on the right-hand side, so-called *surface accumulation/ablation function*, describes another component of the climatic input, the rate of supply of new ice by accumulation, or, conversely the rate at which ice is melted away from the surface.

Mathematically, the problem has a structure of a set of quasi-static (mass & momentum balances) and evolutionary (energy balance) PDEs solved in an evolving geometry (kinematic condition). This makes the problem in its full generality rather challenging both from the analytical and numerical point of view and thus further simplifications are often necessary.

2.2 Shallow ice approximation and beyond

To solve analytically the system of equations governing glacier evolution as presented above is impossible except for several extremely special cases. Consequently, numer-

ical simulations play a critical role in present-day glaciology. Interestingly, even with the capabilities of modern supercomputers, solution of the so-called full-Stokes (or full Stokes-Fourier) model specified above remains challenging especially for long-term and large-scale simulations of ice sheets such as the Antarctic or Greenland ones. In those cases, further simplifications must be imposed that allow one to reduce the computational requirements and to make the computations feasible. For grounded glaciers and ice sheets, i.e. ice masses resting on some bedrock (unlike the floating ice masses - so-called *ice shelves*), the popular and widely employed simplification is based on a formal asymptotic expansion of the system of governing equations in terms of a small parameter - an aspect ratio $\varepsilon{=}\frac{H}{L}$ - expressing the "flatness" of the glacier in terms of a ratio of its characteristic thickness H and its characteristic lateral dimension L. For large glaciers and ice sheets on Earth like the Greenland or Antarctic ice sheet, this parameter is typically $\leq 10^{-2}$.

A particularly important is the zeroth-order limit of this formal asymptotic expansion, so-called *shallow ice approximation (SIA)*, introduced by Hutter (1983) and Morland (1984). It stems from the hydrostatic approximation by assuming $\mathbb{S}_{33} \simeq 0$, which allows one to integrate the vertical component of the momentum balance. SIA further imposes the following a-priori scaling of the extra stress components

$$\mathbb{S}_{xz}, \mathbb{S}_{yz} = O(\varepsilon)\rho_i g H, \qquad \mathbb{S}_{xx}, \mathbb{S}_{yy}, \mathbb{S}_{xy} = O(\varepsilon^2)\rho_i g H\,, \tag{2.6}$$

which means that the vertical shear stresses dominate the longitudinal stresses (and also the horizontal shear stress). Introducing this scaling into the governing equations and taking only the highest-order terms in the power expansion in ε, this set of assumptions allows one to explicitly identify the horizontal shear stress components in a closed form

$$\mathbb{S}_{xz} \simeq -\rho_i g (f^s - z)\frac{\partial f^s}{\partial x}\,, \tag{2.7a}$$

$$\mathbb{S}_{yz} \simeq -\rho_i g (f^s - z)\frac{\partial f^s}{\partial y}\,, \tag{2.7b}$$

proportional to the local surface gradient. A great advantage of the SIA approximation is that it admits a semi-explicit evaluation of the velocity field based on (2.7) by integrating the corresponding tensorial components of Glen's flow law rheology (2.2). This yields in particular the following formulae for horizontal components of the velocity field:

$$\mathbf{v}_x(t,x,y,z) = \mathbf{v}_x^b - 2(\rho g)^n |\nabla_h f^s|^{n-1}\frac{\partial f^s}{\partial x}\int_{f^b}^{z} \mathcal{A}(\vartheta')(f^s - z')^n\, dz'\,, \tag{2.8a}$$

$$\mathbf{v}_y(t,x,y,z) = \mathbf{v}_y^b - 2(\rho g)^n |\nabla_h f^s|^{n-1}\frac{\partial f^s}{\partial y}\int_{f^b}^{z} \mathcal{A}(\vartheta')(f^s - z')^n\, dz'\,, \tag{2.8b}$$

where $\mathbf{v}_x^b$, $\mathbf{v}_y^b$ are the components of velocity at the base, n is the Glen's flow law exponent and $\nabla_h f^s = \left(\frac{\partial f^s}{\partial x}, \frac{\partial f^s}{\partial y}\right)$. The remaining velocity component $\mathbf{v}_z$ can be obtained by integrating the mass conservation (2.1a), and from the complete velocity field, all the remaining stress components can be recovered based on (2.2b).

Consequently the numerical implementation of the mechanical part of the SIA problem becomes matrix-free and thus computationally essentially trivial - limited to one-dimensional (vertical) quadratures. Notably, the evolution equation for the surface topography (2.5), which is originally hyperbolic, admits under the SIA assumptions reformulation to the form

$$\frac{\partial f^s}{\partial t} + \nabla_h \cdot (\mathcal{K}(|\nabla_h f^s|)\nabla_h f^s) = a^s \,. \tag{2.9}$$

If explicit time discretization is employed in the numerical implementation of this equation, and the nonlinear diffusivity $\mathcal{K}(|\nabla_h f^s|)$, is evaluated from the surface slope in the previous time step, the kinematic equation becomes linear parabolic. This of course greatly improves numerical stability of the numerical solution of the geometry evolution. Combination of these performance and stability advantages has led to a great popularity of the SIA and its intense applications especially in the paleo-simulations of large ice sheets, i.e. in simulations spanning hundreds to thousands of milenia (e.g. Hughes, 1981; Holmlund and Fastook, 1995; Ritz et al., 1996; Tarasov and Peltier, 2002; Kirchner et al., 2011; Kusahara et al., 2015; Souček et al., 2015).

The validity of the shallow ice approximation unfortunately relies on the specific scaling assumptions on the components of the stress field (2.6) which become to a lesser or greater extent violated in many important cases (e.g. Ahlkrona et al., 2013). For this reason, the SIA is known to fail in describing for instance *ice streams*, fast flowing regions close to the glacier outlets, whose motion is typically sped up by sliding on a water-lubricated base. It also does not hold for *ice shelves* - floating ice masses where the longitudinal not shear stresses dominate their dynamics. Neither does it describe the *transition zones* between grounded ice sheets and ice shelves which determine the *grounding line dynamics* - a phenomenon which is critical for understanding and predicting destabilization of ice shelves, observed recently with an increasing rate all around the world. Last but not least, the SIA assumptions are problematic in smaller *alpine-type glaciers*, for which the flatness ratio is much higher than for the large ice sheets and the formal asymptotic expansion probably does not make sense.

A remedy in these cases has been sought by a number of different approaches. For instance, by introducing different apriori scaling assumption, a model of the same order of accuracy but yielding different governing equations was designed to capture shallow shelf dynamics - so-called *Shallow Shelf Approximation* (SSA) (Morland,

1987; MacAyeal, 1989). *Hybrid models* have then been designed that combine the SIA with the SSA in order to capture both the grounded and marine ice sheet/ice shelf dynamics (e.g. Pollard and DeConto, 2012). *Higher-order models* have been designed either as formal continuation of the asymptotic expansion corresponding to the SIA (and SSA) such as First or Second-Order SIA (FOSIA, SOSIA) (e.g. Hutter, 1983; Baral et al., 2001). Alternatively, different class of higher-order models has been derived directly from the full Stokes model by neglecting certain terms indicated by scaling but not employing the asymptotic expansion. Most of these models retain the deviatoric stresses neglected in the SIA, the most popular among them is perhaps the Blatter-Pattyn model (Blatter, 1995; Pattyn, 2003), a systematic hierarchy of higher order models has been given in Hindmarsh (2004). Finally, with the increasing computational power of modern computers, full-Stokes models are also being used more and more extensively (e.g. Gillet-Chaulet et al., 2012; Seddik et al., 2012; Rückamp et al., 2022).

A community effort gradually led to a development of a series of benchmark exercises (e.g. Pattyn et al., 2008, 2012, 2013) that have been devised to elucidate the accuracy of the approximate models when compared to the full-Stokes solutions and to quantify the effect of these approximations on phenomena such as the grounding line migration. The higher-order approximation effects have been studied also in the context of thermomechanical instabilities (Souček and Martinec, 2011) or in large-scale paleoglacial simulations (Kirchner et al., 2016). Interestingly, the latter study indicates that the use of second-order SIA, contrary to what has been expected, does not provide a sufficient accuracy improvement compared to the SIA solution. With an alternative such as the Pattyn-Blatter or the full-Stokes model being significantly more demanding in terms of required computational power, suitable alternatives still ought to be looked for.

Iterative improvement of the shallow-ice approximation

In Souček and Martinec (2008), we have aimed at contributing to the search of approximations extending the shallow ice approximation in terms of accuracy but keeping some of its advantages in terms of the lower computational requirements compared to the full-Stokes solution. We devised a relatively simple algorithm (called "SIA-I"), which provides an iterative improvement of the SIA solution in a series of steps whose computational cost is comparably as low as the solution of the SIA itself. The iterative improvement is moreover straightforward implementation-wise, allowing for the technique to be implemented into any existing SIA-based codes. Moreover, as a first iteration the algorithm provides the classical SIA solution. Since the algorithm is used in the appended manuscript [P1], we briefly recapitulate

its basic structure here.

The algorithm is based on the following strategy (assuming isothermal setting for simplicity). We consider the mass, linear momentum and rheology equations characterized formally by operators $\mathcal{A}_{\mathrm{mass}}$, $\mathcal{A}_{\mathrm{lmom}}$, $\mathcal{A}_{\mathrm{rheo}}$ so that these governing equations read

$$\mathcal{A}_{\mathrm{mass}}(\mathbf{v}) = 0\,, \qquad \mathcal{A}_{\mathrm{lmom}}(p, \mathbb{S}) = 0\,, \qquad \mathbb{S} = \mathcal{A}_{\mathrm{rheo}}(\mathbf{v}, p)\,. \tag{2.10}$$

Given an estimate of the fields $\mathbf{v}^k$, p^k, $\mathbb{S}^k$ in a k-th step of the algorithm, we look for increments $\delta\mathbf{v}$, δp, $\delta\mathbb{S}$ such that the exact solution of (2.10) reads

$$\mathbf{v} = \delta\mathbf{v} + \mathbf{v}^k\,, \qquad p = \delta p + p^k\,, \qquad \mathbb{S} = \delta\mathbb{S} + \mathbb{S}^k\,.$$

Linearity of the momentum balance admits to write it as an equation for the increments which, in the algorithm, is replaced by its SIA counterpart. Formally, we consider an incremental linear momentum balance of the form

$$\mathcal{A}^{\mathrm{SIA}}_{\mathrm{lmom}}(\delta p, \delta\mathbb{S}) = -\mathcal{A}_{\mathrm{lmom}}(p^k, \mathbb{S}^k)\,.$$

The left hand side admits a simple inversion by the solution of SIA problem with the given right-hand side. The updated stresses are used to infer an updated velocity field by integrating the rheology equation and the mass balance in a procedure again analogous to the the corresponding SIA step, so written formally, one solves

$$(\mathbf{v}_x^{k+1}, \mathbf{v}_y^{k+1}) = (\mathcal{A}^{\mathrm{SIA}}_{\mathrm{rheo}})^{-1}(\mathbb{S}^k + \delta\mathbb{S}, p^k + \delta p)\,, \qquad \mathbf{v}_z^{k+1} = \mathcal{A}^{-1}_{\mathrm{mass}}(\mathbf{v}_x^{k+1}, \mathbf{v}_y^{k+1})\,.$$

From the velocity field, the remaining components of the stress field (which have not been updated yet) are computed

$$\mathbb{S}^{k+1} = \mathcal{A}_{\mathrm{rheo}}(\mathbf{v}^{k+1}, p^{k+1})\,, \qquad p^{k+1} = p^k + \delta p\,.$$

The process is iterated, and, in order to achieve convergence, certain under-relaxation is performed.

The algorithm was implemented in a Fortran90 code, using the staggered grid finite difference scheme with the vertical coordinate mapped on the actual shape of the ice sheet (essentially an Arbitrary-Langrangian-Eulerian (ALE) approach). The code admits the use of both the Cartesian and the spherical coordinates and includes also the evolution equation for temperature and geometry. The thermo-mechanical coupling aspects have been tested in an evolutionary benchmark exercise EISMINT (Huybrechts and Payne, 1996) (European Ice Sheet Modeling IniTiative) and also in EISMINT Greenland models benchmark focused on long-term large-scale Greenland ice sheet evolution simulation spanning several glacial cycles.

With an implementation of the SIA-I algorithm, we participated in an influential benchmark experiment focused on comparison of the higher-order approaches to the approximations of flow equations ISMIP-HOM (Benchmark experiments for higher-order and full-Stokes ice sheet models), whose results are summarized in Pattyn et al. (2008) (co-authored). Up to an aspect ratio $\varepsilon=\frac{1}{10}$, our algorithm was comparable to the exact full-Stokes solution in terms of accuracy but with the computational requirements reduced by 1-2 orders of magnitude (Souček and Martinec, 2008; Gagliardini and Zwinger, 2008).

2.3 Brief summary of the results in P1 and P2

[P1] - ISMIP-HEINO experiment revisited: Effect of higher-order approximation and sensitivity study

In [P1], we exploited the favorable accuracy-to-speed ratio of the SIA-I algorithm in an attempt to quantify the role of higher-order approximation of the flow equations on modeling thermo-mechanical cyclic instabilities of glaciers - so-called Heinrich events (Heinrich, 1988). In particular, we revisited the ISMIP-HEINO benchmark experiment (Calov et al., 2010), which was designed to capture the essence of this instability by a "binge-purge" mechanism of thermally-triggered sliding at the base of the glacier. Due to enormous computational requirements, none of the participants provided a full-Stokes solution. We recomputed the results of this experiment with and without the iterative improvement of the SIA solution with the goal to assess the importance of higher-order approximation on the formation and characteristics of the instabilities.

In order to interpret the results in view of the apparently large variability of the published numerical solutions of the benchmark exercise, we devised in [P1] a wavelet-type processing strategy of the resulting time series. This tool allowed us to observe that the higher-order approximation of the flow equations plays only a relatively minor role in the experiment compared to the implementational details of the thermo-mechanical coupling. We have concluded that SIA-based models do not, in this case, lack the ability to reproduce Heinrich-type instabilities, but at the same time, we showed that reliable modeling of Heinrich events might be problematic even for full-Stokes solvers and even in terms of just statistical characteristics.

[P2] - A 3 Ga old polythermal ice sheet in Isidis Planitia, Mars: dynamics and thermal regime inferred from numerical modeling

Guidat et al. (2015) (co-authored) have proposed a glaciological interpretation of

a set of geomorphological features located in the region of Isidis Planitia - a large equatorial impact basin on the surface of Mars. In order to verify their hypothesis, in [P2] we have adapted the numerical code introduced above to simulate the conditions on the ancient Mars, approximately 3 Ga ago, and to investigate the glaciation in the region. The idea was based on the previously published results of the Martian global circulation model (GCM) by Madeleine et al. (2009), which showed that during the periods of high obliquity (rotational axis tilt) that are believed to have occurred in Martian history (Laskar et al., 2004), conditions in the Isidis region may have been favorable for ice accumulation and thus glacier formation. Adopting the synthetic accumulation data and surface temperatures from the GCM and supplementing them with the synthetic geothermal heat flux model based on Grott and Breuer (2010), our simulations revealed that a massive ice sheet with the thickness of several kilometers may have formed in the Isidis basin consistently with the ancient climatic conditions. The thermal insulation effect of the ice cover together with the geothermal cold spot in the heat flux model, led in our simulations to reaching the melting point in an ring-like region of the basin. This provided wet-based conditions at a portion of the glacier base and, together with the simulated ice flow pattern, provided support for the interpretation of the present-day observed geomorphological features as the remnants of an ancient subglacial hydrological network and associated glacial relicts.

Tidal deformation of planetary ice shells

3

This chapter focuses on mathematical modeling of tidally induced deformation of outer ice shells of Saturn's moon Enceladus and Jupiter's moon Europa.

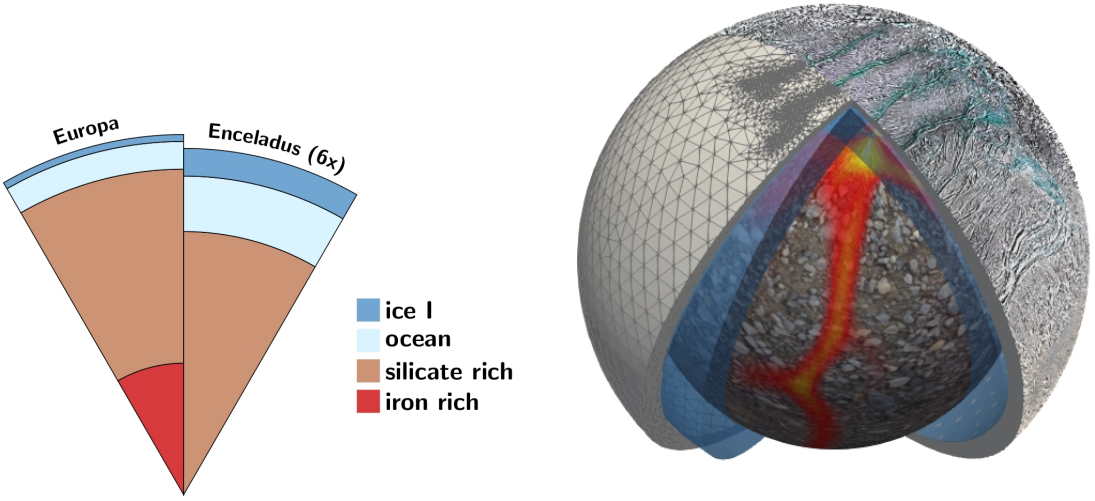

Figure 3.1: Left: A sketch (to scale) of the present day view of the structure of Europa and Enceladus. Right: A visualisation of our mathematical model of Enceladus with the finite element mesh refined in the vicinity of tiger stripes - four prominent faults on the south pole. Enceladus surface image credits NASA/JPL/SSI/USRA/LPI.

For the glaciers and ice sheets discussed in the previous chapter, the primary mode of deformation was the viscous creep which was accommodating gravity induced shear stresses within the ice. In planetary ice shells, such gravity-driven viscous flow analogous to that of glaciers may occur as well in the form of viscous or viscoelastic relaxation of non-equilibrium shapes caused for instance by crater formation (Kihoulou et al., 2022) or by freezing/melting heterogeneities at the interface with the internal ocean (e.g. Ashkenazy et al., 2018; Čadek et al., 2019). Apart from such deformation regime occurring on a geological time scale, another forcing agent is often active, operating on a much shorter - orbital - time scale, whose

importance for the internal and also orbital evolution of these bodies, as well as its role in determining their interior structure, cannot be overestimated - *the tides*.

3.1 Tides on Enceladus and Europa

Both Europa and Enceladus experience forcing due to the tides raised on them by their primaries - Jupiter and Saturn. Tidal forces arise due to a local disbalance between the gravity from the companion body or bodies (primaries in the case of Europa and Enceladus) and the centrifugal force on the adjacent and faraway sides of the moon/planet. Despite the fact that both Europa and Enceladus are locked in the synchronous rotation (i.e. facing their primaries with the same side as our Moon does with respect to the Earth), the tidal potential varies in time due to non-zero eccentricity of the moons' orbits.

These variations of tides induce a periodic forcing on the orbital time scale of days. In response to this short-periodic forcing the moons react by mainly elastic (i.e. reversible) deformation, but inelastic effects attributed to viscoleasticity, plasticity or internal friction arise as well. These cause a phase lag between the tidal forcing and the moons' mechanical response and, more importantly, lead to dissipation of a part of the mechanical energy in the moons' interiors. For Europa and Enceladus, such internal heating source is an important ingredient of their energy budgets, which may be responsible for the creation and sustainability of their liquid oceans, thus making them primary targets of planetary research of prominent astrobiological potential.

Both Europa and Enceladus are differentiated (see the structure in Figure 3.1 (left)) and the tidal response and the associated dissipation in each of the layers differ. Mechanical dissipation in the unconsolidated silicate interior of Enceladus was hypothesized to be the most important source of internal heating for this tiny moon dominating its energy budget (Roberts, 2015; Choblet et al., 2017). On Europa, dissipation in its silicate mantle may be responsible for maintaining volcanic activity until present (Běhounková et al., 2021). Dissipation in the liquid oceans was also considered and modelled (Tyler, 2014; Beuthe, 2016; Matsuyama et al., 2018; Rovira-Navarro et al., 2019) with the conclusion that while it probably plays only a negligible role with the current state of the moons' hydrospheres, its importance may become more profound if the oceans become very thin (for instance as the result of gradual freezing as the bodies cool down). Finally, tidal dissipation in the outer ice shells was suggested to be important (Tobie et al., 2005, 2008; Běhounková et al., 2012), which motivated our own research and led to a series of numerical studies that will be presented after briefly introducing the basic mathematical framework of these

models.

3.2 Mathematical model of tidal deformation and heating

Mechanical part - tidal deformation

The mechanical part of the mathematical model describing tidal deformation of planetary ice shells is represented by a quasi-static equilibrium between the forcing by the disturbing potential V and the deformation of the shell inducing incremental Cauchy stress $\boldsymbol{\sigma}$ (incremental with respect to the reference hydrostatically prestressed state). Unlike the deformation of glaciers with the strains easily exceeding unity, the strains caused by tidal deformation of planetary shells are of the order of 2×10^{-5} for Europa and Enceladus (Tobie et al., 2003; Nimmo et al., 2007). This allows one to neglect the density variations due to volume changes so that the mass balance need not be considered in the problem. The mechanical problem thus reads

$$\operatorname{div}\boldsymbol{\sigma} - \rho_i \nabla V = \mathbf{0}\,, \tag{3.1}$$

where ρ_i denotes ice density and the disturbing potential can be decomposed as

$$V = V^{\text{tidal}} + \delta V^{\text{tidal}}\,. \tag{3.2}$$

The first term represents the exerted (loading) tidal potential by the primary (Saturn or Jupiter) and the second term describes self-gravitation - change of the gravity potential of the moon itself resulting from its deformation by tides. The tidal potential can be approximated, for bodies in a synchronous rotation like Enceladus or Europa, to a first order in eccentricity, by an explicit function of time t, radius r, co-latitude θ and longitude ϕ as follows (Kaula, 1964):

$$V^{\text{tidal}} = r^2\omega^2 e \left\{ \frac{3}{2} P_0^2(\cos\theta)\cos\omega t - \frac{1}{4} P_2^2(\cos\theta)\left[3\cos\omega t\cos 2\phi + 4\sin\omega t\sin 2\phi\right] \right\}, \tag{3.3}$$

where ω is the orbital angular frequency, and P_0^2 and P_2^2 are the associated Legendre functions. For a radially symmetric, isotropic elastic body, which is often a good approximation of the real structure, the self-gravitation effects can be parameterized in terms of potential Love numbers k_ℓ (Love, 1907), relating the induced potential and the loading potential at the surface of the body (r=R) at a given spherical harmonic degree ℓ

$$\delta V_\ell^{\text{tidal}}\Big|_{r=R} = k_\ell \, V_\ell^{\text{tidal}}\Big|_{r=R}\,. \tag{3.4}$$

This expression can be generalized to linear viscoelastic models by replacing the real Love numbers by complex ones. Often the bulk changes in density are negligible and thus the primary self-gravitating effect arises due to deformation of boundaries of the body, i.e. change of shape - the corresponding self-gravitation potential is then sought typically using the Helmert condensation method (e.g. Martinec et al., 1993).

The fact that the tidal deformation is small allows one to formulate the problem in an Eulerian setting but on a fixed undeformed domain on which the effect of shape change is replaced by displacement-dependent boundary conditions. These boundary conditions on the two underformed interfaces of the shell - the upper free surface Γ^{top} and the ice-ocean interface Γ^{bot} can be formulated, after linearization with respect to the displacements, as follows (Souček et al., 2019):

$$\boldsymbol{\sigma}\boldsymbol{n} + \mathbf{u}_r \rho_i g \boldsymbol{n} = \mathbf{0}\,, \qquad \text{at} \qquad \Gamma^{top} \tag{3.5a}$$

$$\boldsymbol{\sigma}\boldsymbol{n} - \mathbf{u}_r (\rho_w - \rho_i) g \boldsymbol{n} = \boldsymbol{n} \rho_w V\,, \qquad \text{at} \qquad \Gamma^{bot}\,. \tag{3.5b}$$

Here $\boldsymbol{n}$ denotes the outer unit normal, ρ_i and ρ_w are the ice and water densities, respectively, g is the (magnitude of) gravity acceleration and $\mathbf{u}_r$ is the radial displacement of the given surface. The terms involving $\mathbf{u}_r$ correspond to the effective weight of the undulated interface and the term on the r.h.s in the second equation represents an incremental pressure in the internal ocean due to tides.

Ice rheology, i.e. the dependence of the incremental Cauchy stress $\boldsymbol{\sigma}$ on the deformation, can on the time scale at which tides operate on Europa and Enceladus (3.55 and 1.37 days, respectively) be often approximated by a Hookean elastic solid. More accurately, linear viscoelastic models for the shear deformation have been introduced to comply with the phase lag between the observed deformation and tidal loading. The two most commonly considered viscoelastic models are the *Maxwell* and *Andrade linear viscoelasticity*. Both models consider viscoelastic response only in the shear component of the deformation, while considering the bulk response of ice as elastic.

The three cases correspond to the following constitutive relations for the incremental Cauchy stress in the time domain (see Section 1.3 for the corresponding expressions in the frequency domain), (Efroimsky, 2012):

- Elastic model

$$\boldsymbol{\sigma} = K \operatorname{div} \mathbf{u} \mathbb{I} + 2\mu \boldsymbol{\varepsilon}^d\,, \tag{3.6a}$$

  Here $\boldsymbol{\varepsilon}^d$ is the deviatoric part of the symmetric gradient of displacement, $\mathbb{I}$ is the identity tensor, and K and μ are the bulk and shear elastic moduli, respectively.

- Viscoelastic models

$$\boldsymbol{\sigma} = K \operatorname{div} \mathbf{u}\mathbb{I} + \mathbb{S}\,, \tag{3.6b}$$

where the deviatoric part of the incremental Cauchy stress $\mathbb{S}$ satisfies

$$2\boldsymbol{\varepsilon}^d = \int_{-\infty}^{t} J(t-\tau)\dot{\mathbb{S}}(\tau,\cdot)d\tau \tag{3.6c}$$

with the compliance J defined as

$$J(t-\tau) = \begin{cases} \frac{1}{\mu}\left(1+\frac{t-\tau}{\tau_M}\right)H(t-\tau) & \text{Maxwell} \\ \frac{1}{\mu}\left(1+\frac{t-\tau}{\tau_M}+\left(\frac{t-\tau}{\zeta_A\tau_M}\right)^{\alpha}\right)H(t-\tau) & \text{Andrade} \end{cases} \tag{3.6d}$$

Here τ_M is the Maxwell time defined as $\tau_M{=}\frac{\eta}{\mu}$ with η denoting ice viscosity, ζ_A and α are parameters and H is the Heaviside function.

Since the deformation induced by tidal forcing is small, ice viscosity in both the Maxwell and Andrade models is sometimes considered to be Newtonian of Arrhenius type (taking into account only diffusion creep out of the four deformation mechanisms described in Section 1.2.2):

$$\eta = \eta_0 \exp\left(\frac{E}{R}\left(\frac{1}{\vartheta}-\frac{1}{\vartheta_b}\right)\right) \tag{3.7}$$

Here E is the activation energy of diffusion creep, R is the universal gas constant, ϑ_b is the temperature at the ice-ocean interface, i.e. local melting point in the interior of Enceladus. The prefactor η_0 represents the lowermost viscosity (viscosity at the melting point), and is a free parameter as it depends on the unknown grain size - typically only some bounds can be inferred from indirect arguments. For example in Čadek et al. (2019), we have shown, that values smaller than $3{\times}10^{14}$ Pa s for Enceladus would be inconsistent with the assumption that the present-day shape of the shell is in a (dynamic) steady state.

Thermal part - heat transfer

The temperature distribution within the shells of icy moons, which strongly affects their viscosity, depends critically on the regime of the heat transfer, mainly on whether or not thermal convection takes place. While convection is considered unlikely for the minuscule Enceladus, the ice shell of much larger Europa probably contains a convecting layer below the upper cold conductive stagnant lid (e.g. Barr and Showman, 2009).

The two cases differ tremendously in terms of the difficulties of coupling the mechanical model of tidal deformation with the thermal evolution of the bodies. In the conductive case, the temperature profile is essentially one-dimensional and can

be relatively simply approximated by an analytical or semi-analytical solution or by a numerical solution of an additional scalar partial differential equation for the temperature. In the latter - convective case - the temperature must be sought for by a numerical solution of the thermo-mechanical equations describing the convecting system. This includes momentum and mass balance for solid state convection, usually formulated in the Boussinesq approximation, see below. Since the thermal convection and the tidal processes occur on very different time scales (millions of years vs. days), some time-scale splitting strategies are in this case necessary. Equations governing the thermal state for the two discussed cases are the following:

Conductive heat transfer

The (steady-state) temperature field ϑ is sought as a solution of stationary heat equation

$$-\operatorname{div}\left(k(\vartheta)\nabla\vartheta\right) = h\,, \tag{3.8}$$

where $k(\vartheta)$ is the heat conductivity considered in the planetary ice shell applications of the form (Petrenko and Whitworth, 2002)

$$k(\vartheta) = \frac{k_0}{\vartheta}\,, \qquad k_0 = 651\mathrm{W\,m^{-1}}\,. \tag{3.9}$$

The internal heating h represents the time-averaged (over the tidal period P) dissipative heating due to the tidal deformation, i.e.

$$h = \frac{1}{P}\int_0^P \mathbb{S} : \mathbb{D}(\mathbf{v}) d\tau\,. \tag{3.10}$$

This system is supplemented with the boundary conditions

$$\vartheta = \vartheta_{\mathrm{melt}} \quad \text{at} \quad \Gamma^{\mathrm{bot}}\,, \qquad \text{and} \qquad \vartheta = \vartheta_{\mathrm{top}} \quad \text{at} \quad \Gamma^{\mathrm{top}}\,, \tag{3.11}$$

specifying the melting temperature $\vartheta_{\mathrm{melt}}$ at the bottom ice-ocean interface Γ^{bot} and the effective surface temperature (given by radiation equilibrium) at the upper surface Γ^{top}.

Convective heat transfer

For a convecting system, the thermal structure is typically sought by solving the coupled system of mass, momentum and heat transfer equations, often considered in the extended Boussinesq approximation (e.g. King et al., 2010):

$$\operatorname{div}\mathbf{v} = 0\,, \tag{3.12a}$$

$$\mathbf{0} = -\nabla p + \operatorname{div}(2\eta\mathbb{D}(\mathbf{v})) - \rho_i\alpha(\vartheta - \vartheta_0)\mathbf{g}\,, \tag{3.12b}$$

$$\rho_0 C_p\left(\frac{\partial\vartheta}{\partial t} + \mathbf{v}\cdot\nabla\vartheta\right) = \operatorname{div}\left(k(\vartheta)\nabla\vartheta\right) + 2\eta|\mathbb{D}(\mathbf{v})|^2 + \rho_0\alpha\vartheta\mathbf{v}\cdot\mathbf{g} + h\,, \tag{3.12c}$$

where $\mathbf{v}$ denotes the convection velocity, p is the dynamic pressure, η the ice viscosity, α the thermal expansion coefficient, ϑ_0 the reference temperature, C_p the heat capacity of ice at constant pressure and tidal heating h is given by (3.10) from the solution of the tidal part of the problem. Thermal boundary conditions can be the same as in the conductive state unless significant melting or freezing takes place at the ice-ocean interface. In that case, alternative Stefan-type boundary condition must be considered, relating the jump of normal heat flux and the melting across the interface and the melting rate, see (4.8). Concerning the linear momentum balance, typically the free-slip boundary conditions are prescribed (see, e.g. King et al., 2010).

3.3 Brief summary of the results in P3–P7

Together with colleagues from the Department of Geophysics and from the Mathematical Institute at the Faculty of Mathematics and Physics, Charles University, and also in collaboration with colleagues from Laboratoire de Planétologie et Géosciences Nantes, France, we have been since 2016 developing a finite-element (FE) code for numerical simulations of tidal deformation of planetary ice shells with Enceladus as the primary target of our research. The core of the code is based on the FEniCS open source FEM library (Alnaes et al., 2015), but currently, it also utilizes external Fortran90 and Python routines for calculation of self-gravitation and for postprocessing of simulation data. The use of finite element spatial discretization allowed us to study the effects of very localized features such as the system of prominent faults - so-called Tiger Stripes - in the south-polar region (SPR) of Enceladus, which is impossible with the more traditional spectral-based methods (e.g. Moore and Schubert, 2000; Tobie et al., 2008). Through the FEniCS library, the code utilizes the computational and MPI parallelization capabilities of PETSc and MUMPS libraries. We have greatly benefited from participation in a series of open access competitions of IT4Innovations National supercomputing center in Ostrava, Czech Republic (`https://www.it4i.cz`). This allowed us to perform evolutionary simulations with up to 10^6-10^7 degrees of freedom.

[P3] - Effect of the tiger stripes on the deformation of Saturn's moon Enceladus

In [P3], we focused on the first-order effects associated with the presence of a system of four prominent faults in the south-polar region (SPR) of Enceladus (see Figure 3.1 (right)) on the tidal deformation of its outer ice shell. Considering for simplicity

a shell of uniform thickness and described by a model of homogeneous isotropic Hookean elastic solid, we modelled the faults as narrow zones of significantly (by 6 orders of magnitude) reduced elastic moduli, passing through the whole shell. As this setting corresponds to frictionless faults (representing a scenario, when the faults are hydrostatically flooded by water from the ocean and/or lubricated by water vapor), it provides an upper estimate of the faults' impact on tidal deformation of the shell. Our results revealed that the stress and deformation field in the SPR in this case becomes dominated by the presence of the faults, which determine both the spatial distribution of these fields and also their magnitude and lead to a several-times fold magnification of tidal displacement in the vicinity of the faults. Consequently, it appears that the tectonic interpretations of SPR geomorphology cannot rely on the traditional spectral-based estimates of the stress field, due to their inability to incorporate the fault's presence.

[P4] - Plume activity and tidal deformation of Enceladus influenced by faults and variable ice shell thickness

In a follow-up study [P4], the effect of presence of faults was combined with a realistic model of the shell thickness variations. The thickness model was based on the study by Čadek et al. (2016) and included significant thinning of the shell in the south-polar region.

We showed that the combined effect of shell thinning and presence of faults in the SPR of Enceladus is synergetic, leading to an increase of the tidal displacement in the SPR by an order of magnitude compared with the case with uniform thickness and without faults. Our calculations were made for an elastic body, but scaling arguments provided maximum estimate of the total tidal heating power due to tidal deformation of the shell for a Maxwell viscoelastic shell. We concluded that deeper heat sources must be present in the interior of Enceladus in order to allow for maintaining a global internal ocean unless the ice viscosity at the base of the shell is unrealistically low. A possible hypothesis was then expressed in a study with our French colleagues (Choblet et al., 2017) (not appended) where we advocate the missing dissipative mechanism to be tidal dissipation in the unconsolidated porous core of the moon. We also showed that while the presence of faults and the shell thickness variations affect the predicted activity of the plume in the SPR of Enceladus, it still cannot explain its observed phase lag.

[P5] - Tidal dissipation in Enceladus' uneven, fractured ice shell

The previous study was extended in [P5] by a series of numerical experiments in which, for the first time, we included also the anelastic effects. We implemented Maxwell viscoelastic rheology with temperature-dependent viscosity and, in addition, we considered also a variant of the Maxwell model tuned to best approximate the Andrade model (in terms of matching the corresponding quality factor). In addition, the conductive temperature equation (3.8) including dissipative heating was solved along with the mechanical system describing tidal deformation and thus the obtained temperature-viscosity-dissipation structure of Enceladus was fully consistent with the mechanical state.

This model allowed us to improve the quantitative prediction of the upper bound of dissipative heat power in the SPR of Enceladus to be 1.1 GW and the total tidal dissipative heating in the whole shell less than 2.1 GW, strengthening the conclusion of our previous paper on the importance of deeper heating sources within Enceladus. A weak point in this study remained in the absence of realistic treatment of friction at the faults themselves, which were still considered as frictionless.

[P6] - Enceladus' tiger stripes as frictional faults: Effect on stress and heat production

A partial remedy with respect to that weak point was achieved in the study [P6]. Here our model was modified in order to allow for quantification of the first order effects of the presence of friction at the faults on the tidal deformation and associated dissipative heating power in the SPR of Enceladus. This was achieved by mimicking Coulomb-type friction at the faults by imposing an effective pseudo-plastic rheology in the narrow fault zones employing effective viscosity of the form

$$\eta_{\text{eff}} = \frac{\eta^*}{\left(1 + \left(\frac{2\eta^* \|\mathbb{D}^d_{\text{visc}}(\mathbf{v})\|}{\sigma_Y}\right)^m\right)^{\frac{1}{m}}} . \tag{3.13}$$

Here η^* represents some auxiliary large background viscosity and $\mathbb{D}_{\text{visc}}$ refers to the viscous (irreversible) part of the viscoelastic deformation and m is a numerical parameter. The yield stress σ_Y depends on the normal stress and on the effective pressure (characterizing equilibrium normal loading of the fault) in such a way, that it drops to zero if the fault is under tension and is of Coulomb-type if under compression. This rheology provides the viscosity equal to the background value η^* for small stresses. With increasing stress, the effective viscosity drops down in such a way that the yield stress σ_Y is never exceeded in the material.

With such a model, we were able to inspect the first-order effects of the inclusion of friction on tiger stripes for a wide range of the friction coefficients. In particular, our study revealed that friction delays the mechanical response of the faults to tidal loading and introduces an asymmetry between the phase of loading and unloading in the normal direction (closing and opening phases). A consequence of this asymmetry is the emergence of certain static background stress in the SPR with a magnitude comparable with the dynamic stresses caused by tides. This effect may have an important impact on the interpretation of Enceladus's SPR tectonics. For the first time in the series of our modeling efforts related to Enceladus, we were also able to provide a quantitative estimate of the frictional heating power due to the strike-slip motions at the faults - a contribution to the energy budget that has been missing in our estimates so far. We concluded that the overall frictional heating power over the tiger stripes probably does not exceed 1 GW. This conclusion further strengthened the hypothesis of other important heating sources in deeper interior of Enceladus in order to counteract the heat losses and allow for the long-term stability of its internal ocean.

[P7] - Tidal walking on Europa's strike-slip faults - insight from numerical modeling

Finally, [P7] is a standalone project standing aside the above series on Enceladus, as it was focused on modeling of tidal deformation on Jupiter's moon Europa. In particular, we have tried to numerically verify a geological hypothesis for the production of lateral offset on fault systems on Europa by a process that has been nicknamed *tidal walking* (Hoppa et al., 1999). In this hypothesis, lateral offset is assumed to gradually accumulate at a fault which is periodically loaded both in normal and tangential direction (with a mutual phase shift), assuming that part of the tangential slip is irreversible as a result of this phase shift.

In order to test this hypothesis, we modelled a cross-section of Europa's shell perpendicular to a preexisting fault. In a Cartesian 2d model, we investigated the regime of deformation due to a periodic strike-slip and normal forcing with the Coulomb-type frictional behavior at the fault while considering viscoelastic Maxwell-type rheology for ice. We focused on studying the role of the phase shift between the strike-slip and normal forcing of the fault and of their amplitudes. We have shown that under favorable conditions, an irreversible slip of the order of several km (i.e. consistent with the observations) may accumulate at the faults over many tidal periods. However, in the model, this required a stress forcing magnitude exceeding the estimated present-day one. On the other hand, such conditions may have been

active in the past history of Europa during epochs of increased eccentricity, making the tidal walking mechanism a plausible explanation of the observed geomorphology. In the model, we also focused on the role of tidal heating by mechanical dissipation on weakening the fault zones and we confirmed that a mechanism of thermal run-away might have been responsible for triggering the tidal walking mechanism. The numerical FE code was again developed in the FEniCS library and was an extension of a code that will be described in more detail in the next chapter in the context of modeling of partial melting and porous media flow in Europa's ice shell.

Melting and melt transport in planetary ice shells 4

In this chapter, we discuss another important physical process influencing planetary ice shell dynamics, modulating the transport of heat and promoting exchange of volatiles - *ice melting/meltwater freezing and the melt transport in ice.*

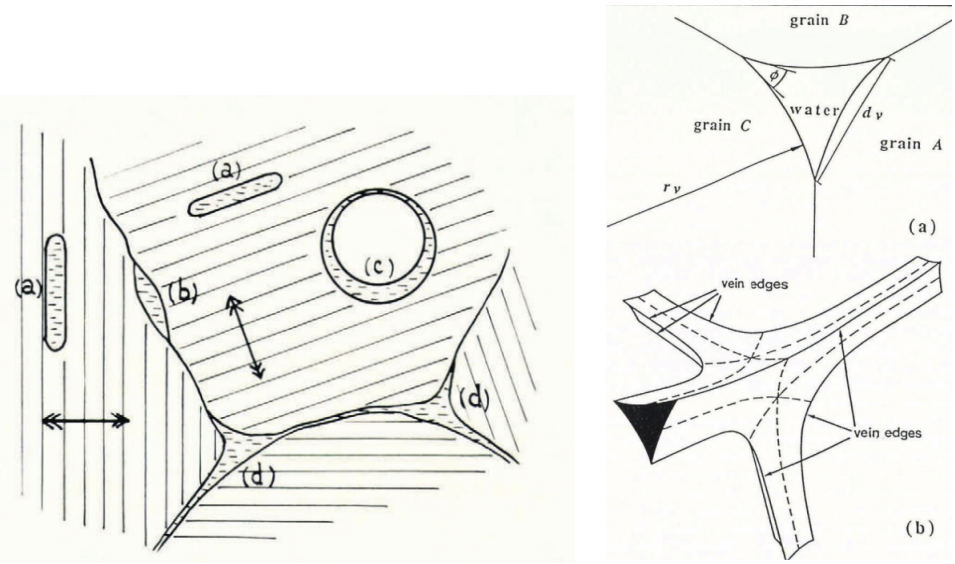

Figure 4.1: Left: Types of liquid water inclusions in polycrystalline ice - (a) intracrystalline, (b) two-grain intersection, (c) air bubbles, (d) three-grain intersection inclusions. From Lliboutry (1971). Right: Detailed sketch of a three-grain intersection, from Mader (1992) after Nye (1989).

In the outer ice shells of icy moons like Enceladus or Europa, melting and freezing occurs primarily in two contexts. For moons with internal oceans a phase change takes place at the interfaces between the ice layers and the oceans as a result of local imbalance between the heat outflux from the ocean and its extraction rate by conduction or convection in the ice layer. The thermo-mechanical coupling between the phases and the evolution of their mutual interface involve solution of the so-called *Stefan problem* or its more involved generalizations (see e.g. König-Haagen et al. (2017)). The shell thickness variations induced by melting/freezing may drive

large scale viscous flow within the shells, salinity variations associated with phase change may dominate internal ocean dynamics (e.g. Soderlund et al., 2014; Kvorka et al., 2018; Ashkenazy et al., 2018; Ashkenazy and Tziperman, 2020).

Alternatively, meltwater may be produced also in the bulk of the shell, for instance at tidally loaded strike-slip faults on Europa, as a result of frictional heating (Nimmo and Gaidos, 2002), or in the low-viscosity regions of ascending plumes several kilometers below the surface as a result of enhanced tidal heating (Sotin et al., 2002; Tobie et al., 2003). The process of near subsurface phase change has been hypothesized as a possible explanation for a number of geomorphological features on icy moons, such as the double ridges (Dombard et al., 2013) or chaos terrain (Schmidt et al., 2011) on the surface of Europa. A critical question in these scenarios concerns stability of such subsurface water reservoirs, which is closely connected with the time scale for which the meltwater "pockets" or lenses could persist as there are at least two mechanisms possibly triggering their instability and draining meltwater away from the surface.

The first one is caused by the negative buoyancy of meltwater with respect to the surrounding ice (for the outer ice I layers) which tends to form *Rayleigh-Taylor instability*, the resulting turnover driving the melt downwards. The second mechanism is related to ice *permeability* - as the ice matrix starts melting and the volume fraction of meltwater increases, after reaching a threshold of a few percent, the matrix becomes permeable to water which then gets drained by *porous flow* in the direction of effective pressure gradient (downwards for outer ice I layers).

Interestingly, these mechanisms of meltwater drainage are very different from the one we observe in terrestrial glaciers. The reason is that on Earth the hydraulic channel and crevasse system is typically open from above where the meltwater is primarily produced and from where it penetrates downwards by the process of hydrofracturing (Fountain and Walder, 1998). In the case of planetary ice shells, the surface is typically very cold ($<$100 K for Europa and $\sim$ 60 K for Enceladus) so no liquid water is present on the surface. So with a possible exception of Enceladus' tiger stripes - south-polar faults penetrating probably the whole shell, most meltwater in the interior of the icy moons' shells is separated from the surface by a layer of impermeable compact solid ice.

As a consequence, the permeability-driven water transport in partially molten regions of the ice layers occurs by a process analogous to silicate melt transport in the Earth's mantle (e.g. McKenzie, 1984; Spiegelman and McKenzie, 1987). Melt transport follows Darcy-type dynamics, but in contrast with the traditional near-subsurface terrestrial porous media hydrology, here, an additional mechanical coupling between the surrounding matrix and the flow of the melt is present. This

coupling results from the fact that extraction of the melt from the matrix must be accompanied by deformation of the matrix material filling the space evacuated by the outflowing melt. This results in an emergence of the so-called *compaction pressure* enriching the Darcy-type flow dynamics and bringing in additional dependence of the flow also on the matrix properties such as its viscosity.

4.1 Mathematical model - porous flow of water in temperate ice

In addressing the meltwater transport in planetary ice shells, we employ the mathematical model of meltwater flow in a viscously deforming temperate ice (i.e. ice at the melting point). The system of governing equations comprises two balances of mass and two balances of linear momentum for the two phases and, since both phases have the same equilibrium melting point temperature, only one energy balance for the mixture as a whole.

The system of governing equations can be derived from the first principles of the theory of multicomponent interacting continua (Drew and Passman, 1998; Bercovici et al., 2001; Šrámek et al., 2007). After model reduction by problem-tailored scaling arguments, the system can be recast to the following form, closely resembling the traditional two-phase equations of melt propagation in silicates, well established in Earth mantle dynamics (McKenzie, 1984; Spiegelman and McKenzie, 1987):

- Balances of mass:

$$\frac{\partial \phi}{\partial t} + \operatorname{div}(\phi \mathbf{v}_f) = \frac{r}{\rho_f}\,, \tag{4.1a}$$

$$\operatorname{div} \mathbf{v}_m + \operatorname{div}(\phi(\mathbf{v}_f - \mathbf{v}_m)) = r\left(\frac{1}{\rho_f} - \frac{1}{\rho_m}\right)\,. \tag{4.1b}$$

  Here ϕ denotes porosity (i.e. volume fraction of fluid), $\mathbf{v}_f$ and $\mathbf{v}_m$ denote the fluid and matrix velocities, respectively, r denotes the melting/freezing rate (positive for melting) and ρ_f, ρ_m are the fluid and matrix (constant) densities, respectively.

- Balances of linear momentum

$$c(\phi)(\mathbf{v}_f - \mathbf{v}_m) = -\phi\left(\nabla \Pi + (\rho_m - \rho_f)\mathbf{g}\right)\,, \tag{4.2a}$$

$$\nabla \Pi = -\phi(\rho_m - \rho_f)\mathbf{g} - \nabla((1-\phi)\mathcal{P}) + \operatorname{div}\left(2(1-\phi)\eta_m \mathbb{D}^d(\mathbf{v}_f)\right)\,. \tag{4.2b}$$

Here Π is the dynamic pressure (defined as the total matrix pressure minus the hydrostatic pressure), $\mathbf{g}$ is the gravity acceleration, η_m matrix shear viscosity given in the considered applications by the effective viscosity (1.10) and $\mathcal{P}$ is the compaction pressure defined as (Bercovici et al., 2001)

$$\mathcal{P} = -\frac{\eta_m}{\phi} \operatorname{div} \mathbf{v}_m \,. \tag{4.3}$$

The symbol $c(\phi)$ denotes the drag coefficient, related to matrix permeability $\kappa(\phi)$ through

$$c(\phi) = \frac{\eta_f \phi^2}{\kappa(\phi)} \,, \qquad \text{where typically} \quad \kappa(\phi) = \kappa_0 \phi^n \,, \tag{4.4}$$

with n between 2 and 3 (e.g. Golden et al., 2007). Sometimes a *percolation threshold* ϕ_c is introduced (Golden et al., 1998), such that the matrix permeability drops by orders of magnitude (or to zero) for $\phi<\phi_c$, while for $\phi\geq\phi_c$, it follows a power-law relationship as in $(4.4)_2$.

- Balance of energy

$$\begin{aligned} &\phi C_f \left(\frac{\partial \vartheta}{\partial t} + \mathbf{v}_f \cdot \nabla \vartheta \right) + (1-\phi) C_m \left(\frac{\partial \vartheta}{\partial t} + \mathbf{v}_m \cdot \nabla \vartheta \right) + Lr \\ &= \operatorname{div} \left(k(\phi) \nabla \vartheta \right) + h + c(\phi) |(\mathbf{v}_f - \mathbf{v}_m)|^2 + (1-\phi) \boldsymbol{\sigma}_m : \mathbb{D}^d(\mathbf{v}_m) - (1-\phi) \mathcal{P} \operatorname{div} \mathbf{v}_m \,, \end{aligned} \tag{4.5}$$

where C_f and C_m are the heat capacities of the two phases, h are external heat sources and $k(\phi)$ is the heat conductivity of the two-phase porous medium given by an implicit relation (Budiansky, 1970; McKenzie, 1984)

$$\frac{\phi}{2 + \frac{k_f}{k}} + \frac{1-\phi}{2 + \frac{k_m}{k}} = \frac{1}{3} \,, \tag{4.6}$$

where k_f and k_m are the fluid and matrix heat conductivities, respectively.

The above system is relatively complex so few comments are perhaps in order. First, let us mention that in the vanishing melt limit, i.e. for $\phi\to 0+$, and in the absence of phase change, i.e. for $r=0$, the above system reduces to the standard incompressible Stokes-Fourier system for the viscous ice matrix.

If melt is present, its transport is given by a Darcy-type equation (4.2a). This equation represents a mechanical quasi-static equilibrium between the drag force caused by the flow (l.h.s. of (4.2a)) and the gradient of dynamic pressure and the gravity force (r.h.s. of (4.2a)). Melt transport and phase change may lead to volume changes of the matrix as the pores close or open and porosity changes accommodating the flow and melting/freezing. These two phenomena are captured by the

mass balances (4.1). The non-zero divergence of the matrix velocity introduces an additional coupling in both mechanical equations through the presence of the compaction pressure $\mathcal{P}$ in (4.2b), expressing the dynamic difference of pressure in the two phases. This difference is related to the compaction of the matrix through a "singular" effective bulk viscosity $\frac{\eta}{\phi}$. Through the dynamic pressure Π, the compaction pressure $\mathcal{P}$ in turn affects the melt separation in (4.2a). The energy balance (4.5) describes an advective transport of heat by both phases (first two terms on the l.h.s. of (4.5)) and the latent heat exchange (last term on the l.h.s. of (4.5)), which are balanced by (in the order in which they appear on the r.h.s. of (4.5)): heat diffusion by Fourier law, external heat sources, mechanical dissipation due to friction between the flowing melt and the matrix, mechanical dissipation by shear deformation of the matrix and mechanical dissipation by bulk deformation of the matrix.

Numerical solution of the above system is non-trivial for many reasons. For instance, in addition to a Stokes-type problem for matrix deformation with nonlinear matrix viscosity, it contains a hyperbolic equation for porosity transport. Since the porosity field may exhibit very steep spatial gradients, preventing spurious oscillations is challenging for most numerical approaches. Another challenge is that the divergence of the matrix velocity is constrained by a non-trivial term. Next, the compaction pressure involves an expression $\frac{\operatorname{div}\mathbf{v}_m}{\phi}$, which is regular for $\phi \to 0+$, but switching between the partially molten and the cold-ice regime requires special treatment. Last but not least, presence of the compaction pressure induces a small-scale pattern formation - creation of so-called *porosity waves* (see e.g. Scott and Stevenson, 1984; Spiegelman, 1993), whose presence tremendously increases the resolution requirements both in space and time. The wavelength of the porosity waves is related with the *compaction length* given by

$$\delta = \sqrt{\frac{\kappa(\phi)\left(\zeta_m + \frac{4}{3}\eta_m\right)}{\eta_f}}\,, \tag{4.7}$$

with $\zeta_m = \frac{\eta_m}{\phi}$ being the effective bulk viscosity of the matrix. In practical applications, the above system is often further simplified in a number of ways. For instance *small porosity approximation* or so-called *zero compaction length limit* have been formulated (e.g. Scott and Stevenson, 1989; Spiegelman, 1993), or a *compaction Boussinesq approximation* (Schmeling, 2000), to name a few.

4.2 Brief summary of the results in P8–P11

Since 2014, with colleagues from the Department of Geophysics and from LPG Nantes, we have been developing finite-element based numerical tools for solution of the above system in the context of partial melting in the interiors of shells of icy moons. The presented calculations were implemented in Fortran90 codes and in an open source finite element platform FEniCS (Alnaes et al., 2015).

[P8] - Water transport in planetary ice shells by two-phase flow - a parametric study

In [P8], we have derived the two-phase formalism (i.e. the themo-mechanical governing equations) for ice-water mixture within planetary ice shells. In this regard, we followed the well-established methodology stemming from the works of Drew and Passman (1998); Bercovici et al. (2001); Šrámek et al. (2007), which starts from the general framework of the two-phase continuum balance equations for mass, momentum, and energy. By employing also the entropy balance and the second law of thermodynamics, constitutive relations are identified in the spirit of linear irreversible thermodynamics (de Groot and Mazur, 1984). We performed a non-dimenzionalization and scaling analysis of the final system of governing equations and by introducing a scaling tailored for the ice shell of Europa, we arrived at the reduced model.

For this model, in a simplified one-dimensional geometry, we investigated numerically how the model parameters affect the character of downward gravity driven extraction of meltwater by porous flow. We focused on the role of permeability (porosity exponent and permeability prefactor, percolation threshold, background porosity), ice rheology (composite vs. simple, temperature effects, porosity weakening), surface tension and compaction length. We confirmed numerically that the most critical parameter with respect to the determination of the melt extraction time scale is the ice permeability, while the other parameters played a minor role. Interestingly, a reasonable approximation of the extraction time scale was obtained also when the mechanical coupling between the two phases was neglected in the so-called zero compaction length limit. The spatial character of the melt flow was very sensitive to the compaction length. The cases with small compaction length produced highly oscillatory porosity wave trains, while the zero compaction length limit case produced a single propagating porosity discontinuity. A correspondence between the two cases could only be established in a weaker sense of spatial averages, indicating possible relationship in the context of generalized solutions (in the

sense of distributions).

[P9] - Ice melting and downward transport of meltwater by two-phase flow in Europa's ice shell

In [P9], we applied the two-phase model established in [P8] in a study of the stability of shallow subsurface meltwater reservoirs in the outer ice shell of Jupiter's moon Europa. We considered in particular two scenarios for the formation of observed surface geomorphological features, which both have been associated with hypotheses involving near-subsurface melting: (i) *Chaos terrains* resulting from melting in the heads of ascending ice plumes and (ii) *double ridges* forming as a results of melting at tidally loaded strike-slip faults within the shell.

We employed a simplified one-dimensional setting of the porous flow equations described above and we solved the system numerically using a combination of finite element and finite volume techniques implemented in a Fortran90 code (Kalousová, 2014). We showed that within the ascending plumes, any meltwater formed at their heads would be transported very rapidly (on the time scale of $\leq$100 kyr) to the internal ocean by the mechanism of two-phase flow in the form of porosity waves. Consequently, long-term stability of meltwater pockets in ascending plumes was shown to be unlikely. On the other hand, our simulations indicated that stable (over Myr) meltwater reservoirs could exist in connection with the strike-slip faults underlain by cold impermeable ice. This identified the double ridges - ubiquitous geomorphological features on Europa's surface - as the potential candidates for the detection of shallow subsurface water lenses by ice-penetrating radar instrument in future satellite missions to the Jovian system.

[P10] - Water generation and transport below Europa's strike-slip faults

In the follow-up study [P10], we revisited the favorable case (from the point of view of water stability) - the strike-slip faults - using a two-dimensional Cartesian finite element model for the water-ice system in an impermeable limit, which we implemented in the FEniCS library Alnaes et al. (2015). This allowed us to further constrain the meltwater extraction time scale and to estimate the amount of accumulated stable subsurface meltwater. Contrary to the one-dimensional case, the 2d simulations allowed us to incorporate and to quantify the melt extraction effectiveness of another mechanism - formation of Rayleigh-Taylor instabilities, caused by the density contrast between water and ice.

In our simulations, the Rayleigh-Taylor instabilites formed typically withing several Myr, draining efficiently the melt downwards and thus preventing formation of totally molten shallow subsurface reservoirs (water lenses). Consequently, the maximum predicted meltwater volume fraction rarely exceeded 10%. Interestingly, by evaluating the volume changes associated with ice melting, meltwater transport and refreezing, we were able to predict formation of surface topography above the strike slip faults consistent with the observed characteristics of the double ridges.

[P11] - Semi-analytical benchmark for the Stefan problem - assessing accuracy of enthalpy-based methods

Paper [P11] is a slightly standalone project, where we investigated melting of ice from a different perspective. Alternatively to the cases described above, where the melt was produced within the ice matrix and transported by porous flow, melting or freezing can also occur at the phase-change interface between the ice layer and the internal ocean. Here, the primary role is played by the so-called Stefan condition - local surface energy or enthalpy balance - which relates the jump in the normal heat flux from the two sides of the interface and the rate at which melting/freezing occurs:

$$L\rho_i(\mathbf{v}-\boldsymbol{\nu})\cdot\boldsymbol{n} = (\mathbf{q}_i - \mathbf{q}_o)\cdot\boldsymbol{n}\,, \tag{4.8}$$

here L is the latent heat of melting, ρ_i the ice density, $\mathbf{v}$ the material velocity of ice at the interface and $\boldsymbol{\nu}$ is the velocity of the interface. The left hand side of (4.8) thus expresses the rate of mass flux through the interface (i.e. melting/freezing rate) multiplied by the latent heat. This is equal to the difference between the normal heat influx into ice and $\mathbf{q}_i\cdot\boldsymbol{n}$ heat outflux from the ocean $\mathbf{q}_o\cdot\boldsymbol{n}$, where $\boldsymbol{n}$ denotes the unit normal to the interface.

When designing a computational strategy to solve the thermomechanical evolution of the two phases coupled thermally by the Stefan condition, as a first step, we focused on development of a robust and reliable testing methodology. In [P11], we devised a semi-analytical benchmark experiment for conductive radially symmetric Stefan problem in arbitrary dimension, i.e. for the situation when the two subdomains adjacent to the phase change interface are purely conductive single-component media (e.g. water and ice) with the heat conductivities given by Fourier's law.

We were interested in a comparison of two standard *enthalpy formulations* of the energy balance, that allow one to avoid explicit tracking of the phase change interface while incorporating the latent heat of melting/freezing. This feature makes the enthalpy methods particularly suitable for applications involving coupling of phase change with the flow of one or both phases. By implementing the methods in

a finite-element setting using the FEniCS library Alnaes et al. (2015), we studied also the stability of the methods with respect to the choice of discretization parameters. Our results allowed us to inspect the trade-off between the spatial and temporal resolution and the temperature scale characterizing the "width" of the smeared (diffuse interface) transition between the two phases. The computational code was made public as a testbed for benchmarking other computational approaches to the Stefan problem.

Conclusions and future outlooks 5

In this thesis and in the appended papers, I summarized a portion of my research dedicated to three different fields of computational geophysics unified by the material involved in the processes - water ice. I believe that together with my colleagues, we have contributed to all these three branches on a general level by development of novel modeling approaches that have been previously missing in the fields. This was accompanied by designing dedicated numerical tools and, by using these tools in particular applications, also by addressing a number of challenging physical questions through often extensive computer simulations.

In all of the three geophysical fields I am still active at present and in each of them I intend to pursue new scientific goals. Let me mention some of the current short and mid-term ones.

Concerning the topic of *gravity driven glacial flows*, we have recently revived the collaboration with the geological/geomorphological group in LPG Nantes (Stéphane Pochat and Olivier Bourgeois) with the goal to reconstruct the glaciation during the last glacial maximum (LGM) in the Massive Central region in Cantal, France. The new field data mapping the extent of the LGM extent that have been gathered recently by the French colleagues, have confirmed our earlier preliminary modeling results. With these data, we have gained tools to better constrain the climatic input and to simulate the last ice age glacier growth in the region followed by the successive deglaciation.

Concerning the topic of *partial melting and porous flow* - we have an on-going and long-lasting project with Dr. Klára Kalousová from the Department of Geophysics, focused on the incorporation of the effect of salts into her two-phase code with an application to the transport processes within planetary ice shells. Salts (like NaCl, $MgSO_4$) play a significant role in the dynamics of these layers due to their antifreezing effect and could dramatically change our view of the conditions for existence of shallow subsurface water reservoirs on bodies like Europa. The incorporation of salts is a challenging task both from the modeling point of view and also from the point of view of numerical approach. It will require to reformulate our current two-phase single-component formalism to a two-phase two-component formalism. In this di-

rection, we have already developed the mathematical and physical model using the enthalpy-based approach and we have also implemented it within the finite-element FEniCS environment. Currently we are extensively testing the numerical tool. In another project with my Ph.D. student, Jiří Malík, we have recently developed a finite-element numerical tool that allows us to couple the motion of a rigid-obstacle which serves as a heat source and is immersed in a thermo-mechanically evolving two-phase ice-water environment. The target application here are numerical simulations of the operation of cryobots - ice penetrating instruments planned to melt through planetary ice shells on Europa and possibly Enceladus and reach and sample their internal oceans. We are currently in the phase of testing the numerical tool.

The core of my current geophysical research remains in further development of the finite-element framework for *modeling planetary ice shells of Europa and primarily, of Enceladus* in collaboration with Dr. Marie Běhounková from the Department of Geophysics. With the Enceladus Orbilander recently identified as the second highest priority NASA Flagship mission for the upcoming decade by the Solar System Decadal Survey committee, we plan to further intensify our goals mainly in the following directions:

- Studying the *dynamic evolution of Enceladus's ice shell shape* by coupling the heat transfer through the internal ocean and the ice shell via Stefan condition (phase change interface evolution) and computing the associated large scale viscous flow within the shell. With the huge temperature-induced viscosity contrast across the shell, and given the shell thickness variations, this process cannot be studied with the traditional spectral based methods and requires the use of tailored techniques such as the FEM approach developed in our group.

- The internally-driven shape evolution of the shell is expected to have an impact on the *global rotational dynamics* of the whole moon and might even trigger its dynamic reorientation. We intend to study the process and to assess its importance for Enceladus and other icy moons by coupling the above internal dynamics FEM tool with the polar wander numerical code developed in the group at the Department of Geophysics.

- By employing more advanced descriptions of ice rheology in combination with the free-surface evolution, we plan to study *surface geomorphologic signatures of the internal dynamics* of icy moons. This involves studying of damage-induced fracture initiation within the shell - a proof of work has been done in this direction during a bachelor project of my student Daniel Broško, where we

confirmed the capacity of the deformation driven damage mechanics suggested by Duddu and Bassis (2020) to serve as a continuum alternative to linear elastic fracture mechanics. We intend to study the process of tiger stripes formation on Enceladus with this approach. Alternatively, by adopting into our two-phase flow model (Kalousová et al., 2016) the near-surface plasticity and the free surface evolution by a methodology tested in Kihoulou et al. (2022), we also plan to revisit our hypothesis on the origin of double ridges on Europa by subsurface melting at the strike-slip faults and subsequent freezing of percolated meltwater, articulated in Kalousová et al. (2016).

Bibliography

J. Ahlkrona, N. Kirchner, and P. Lötstedt. A numerical study of scaling relations for non-newtonian thin-film flows with applications in ice sheet modelling. *The Quarterly Journal of Mechanics and Applied Mathematics*, 66(4):417–435, 08 2013. ISSN 0033-5614. doi: 10.1093/qjmam/hbt009.

M. S. Alnaes, J. Blechta, J. Hake, A. Johansson, B. Kehlet, et al. The FEniCS Project Version 1.5. *Archive of Numerical Software*, 3(100):9–23, 2015. doi: https://doi.org/10.11588/ans.2015.100.20553.

Y. Ashkenazy and E. Tziperman. Europa's dynamic ocean: Taylor columns, eddies, convection, ice melting and salinity. In *European Planetary Science Congress*, pages EPSC2020–538, September 2020. doi: 10.5194/epsc2020-538.

Y. Ashkenazy, R. Sayag, and E. Tziperman. Dynamics of the global meridional ice flow of Europa's icy shell. *Nature Astronomy*, 2:43–49, December 2018. doi: 10.1038/s41550-017-0326-7.

D.R. Baral, K. Hutter, and R. Greve. Asymptotic Theories of Large-Scale Motion, Temperature, and Moisture Distribution in Land-Based Polythermal Ice Sheets: A Critical Review and New Developments. *Applied Mechanics Reviews*, 54(3): 215–256, 05 2001. ISSN 0003-6900. doi: 10.1115/1.3097296.

A. C. Barr and A. P. Showman. Heat transfer in europa's icy shell. In R. T. Pappalardo, W. B. McKinnon, and K. Khurana, editors, *Europa*, pages 405–430. The University of Arizona Press, Tucson, 2009.

A.C. Barr and W.B. McKinnon. Convection in ice I shells and mantles with self-consistent grain size. *J. Geophys. Res.*, 112:2012, 2007. doi: 10.1029/2006JE002781.

D. Bercovici, Y. Ricard, and G. Schubert. A two-phase model for compaction and damage: 1. general theory. *Journal of Geophysical Research: Solid Earth*, 106 (B5):8887–8906, 2001. doi: https://doi.org/10.1029/2000JB900430.

M. Beuthe. Crustal control of dissipative ocean tides in Enceladus and other icy moons. *Icarus*, 280:278–299, 2016. doi: 10.1016/j.icarus.2016.08.009.

H. Blatter. Velocity and stress fields in grounded glaciers: a simple algorithm for including deviatoric stress gradients. *Journal of Glaciology*, 41(138):333–344, 1995. doi: 10.3189/S002214300001621X.

G. S. Boulton and R. C. A. Hindmarsh. Sediment deformation beneath glaciers: Rheology and geological consequences. *Journal of Geophysical Research: Solid Earth*, 92(B9):9059–9082, 1987. doi: https://doi.org/10.1029/JB092iB09p09059.

B. Budiansky. Thermal and thermoelastic properties of isotropic composites. *Journal of Composite Materials*, 4(3):286–295, 1970. doi: 10.1177/002199837000400301.

M. Běhounková, G. Tobie, G. Choblet, and Čadek. Tidally-induced melting events as the origin of south-pole activity on Enceladus. *Icarus*, 219:655–664, 2012. doi: 10.1016/j.icarus.2012.03.024.

M. Běhounková, G. Tobie, G. Choblet, and O. Čadek. Impact of tidal heating on the onset of convection in Enceladus's ice shell. *Icarus*, 226:898–904, 2013. doi: 10.1016/j.icarus.2013.06.033.

M. Běhounková, G. Tobie, O. Čadek, G. Choblet, C. Porco, et al. Timing of water plume eruptions on Enceladus explained by interior viscosity structure. *Nat. Geosci.*, 8:601–604, August 2015. doi: 10.1038/ngeo2475.

M. Běhounková, G. Tobie, G. Choblet, M. Kervazo, M. Melwani Daswani, et al. Tidally induced magmatic pulses on the oceanic floor of jupiter's moon europa. *Geophys. Res. Let.*, 48(3):e2020GL090077, 2021. doi: 10.1029/2020GL090077.

R. Calov, R. Greve, A. Abe-Ouchi, E. Bueler, P. Huybrechts, et al. Results from the ice-sheet model intercomparison project–heinrich event intercomparison (ismip heino). *Journal of Glaciology*, 56(197):371–383, 2010. doi: 10.3189/002214310792447789.

J. C. Castillo-Rogez, M. Efroimsky, and V. Lainey. The tidal history of Iapetus: Spin dynamics in the light of a refined dissipation model. *J. Geophys. Res. Planets*, 116(E9):E09008, September 2011. doi: 10.1029/2010JE003664.

G. Choblet, G. Tobie, C. Sotin, M. Běhounková, O. Čadek, et al. Powering prolonged hydrothermal activity inside Enceladus. *Nat. Astron.*, 1:841–847, 2017. doi: 10.1038/s41550-017-0289-8.

O. Čadek, G. Tobie, T. van Hoolst, M. Masse, G. Choblet, et al. Enceladus's internal ocean and ice shell constrained from cassini gravity, shape, and libration data. *Geophys. Res. Let.*, 46:5653–5660, 2016. doi: 10.1002/2016GL068634.

O. Čadek, O. Souček, M. Běhounková, G. Choblet, G. Tobie, et al. Long-term stability of Enceladus' uneven ice shell. *Icarus*, 319:476–484, 2019. ISSN 0019-1035. doi: https://doi.org/10.1016/j.icarus.2018.10.003.

D. Dahl-Jensen and N. Gundestrup. Constitutive properties of ice at dye 3 greenland. In E. D. Waddington and J. S. Walder, editors, *The physical basis of ice sheet modelling*, IAHS, pages 31–43, 1987.

S.R. de Groot and P. Mazur. *Non-equilibrium Thermodynamics*. Dover Books on Physics. Dover Publications, 1984. ISBN 9780486647418.

S. De La Chapelle, H. Milsch, O. Castelnau, and P. Duval. Compressive creep of ice containing a liquid intergranular phase: Rate-controlling processes in the dislocation creep regime. *Geophysical Research Letters*, 26(2):251–254, 1999. doi: https://doi.org/10.1029/1998GL900289.

A.J. Dombard, G.W. Patterson, A.P. Lederer, and L.M. Prockter. Flanking fractures and the formation of double ridges on europa. *Icarus*, 223(1):74–81, 2013. doi: https://doi.org/10.1016/j.icarus.2012.11.021.

D.A. Drew and S.L. Passman. *Theory of Multicomponent Fluids*. Springer, New York, 1998.

S. Duddu, R. Jiménez and J. Bassis. A non-local continuum poro-damage mechanics model for hydrofracturing of surface crevasses in grounded glaciers. *Journal of Glaciology*, 66(257):415–429, June 2020. doi: 10.1017/jog.2020.16.

G. Durand, J. Weiss, V. Lipenkov, J.M. Barnola, G. Krinner, et al. Effect of impurities on grain growth in cold ice sheets. *Journal of Geophysical Research: Earth Surface*, 111(F1), 2006. doi: https://doi.org/10.1029/2005JF000320.

W. B. Durham, L. A. Stern, and S. H. Kirby. Rheology of ice i at low stress and elevated confining pressure. *Journal of Geophysical Research: Solid Earth*, 106 (B6):11031–11042, 2001. doi: https://doi.org/10.1029/2000JB900446.

W. B. Durham, O. Prieto-Ballesteros, D. L. Goldsby, and J. S. Kargel. Rheological and thermal properties of icy materials. *Space Science Reviews*, 153(1):273–298, 2010. doi: 10.1007/s11214-009-9619-1.

M. Efroimsky. Tidal Dissipation Compared to Seismic Dissipation: In Small Bodies, Earths, and Super-Earths. *ApJ*, 746:150, February 2012. doi: 10.1088/0004-637X/746/2/150.

A. G. Fountain and J. S. Walder. Water flow through temperate glaciers. *Reviews of Geophysics*, 36(3):299–328, 1998. doi: https://doi.org/10.1029/97RG03579.

O. Gagliardini and T. Zwinger. The ismip-hom benchmark experiments performed using the finite-element code elmer. *The Cryosphere*, 2(1):67–76, 2008. doi: 10.5194/tc-2-67-2008.

F. Gillet-Chaulet, O. Gagliardini, H. Seddik, M. Nodet, G. Durand, et al. Greenland ice sheet contribution to sea-level rise from a new-generation ice-sheet model. *The Cryosphere*, 6(6):1561–1576, 2012. doi: 10.5194/tc-6-1561-2012.

J. W. Glen. Experiments on the deformation of ice. *Journal of Glaciology*, 2(12): 111–114, 1952. doi: 10.3189/S0022143000034067.

J.W. Glen and M.F. Perutz. The creep of polycrystalline ice. *Proceedings of the Royal Society of London. Series A. Mathematical and Physical Sciences*, 228(1175):519–538, 1955. doi: 10.1098/rspa.1955.0066.

K. M. Golden, H. Eicken, A. L. Heaton, J. Miner, D. J. Pringle, et al. Thermal evolution of permeability and microstructure in sea ice. *Geophysical Research Letters*, 34(16), 2007. doi: https://doi.org/10.1029/2007GL030447.

K.M. Golden, S.F. Ackley, and V.I. Lytle. The percolation phase transition in sea ice. *Science*, 282(5397):2238–2241, 1998. doi: 10.1126/science.282.5397.2238.

D. L. Goldsby and D. L. Kohlstedt. Superplastic deformation of ice: Experimental observations. *J. Geophys. Res.*, 106:11017–11030, 2001. doi: 10.1029/2000JB900336.

R. Greve and H. Blatter. *Dynamics of Ice Sheets and Glaciers*. Advances in Geophysical and Environmental Mechanics and Mathematics. Springer Berlin, Heidelberg, 2009. ISBN 978-3-642-03414-5.

M. Grott and D. Breuer. On the spatial variability of the martian elastic lithosphere thickness: Evidence for mantle plumes? *Journal of Geophysical Research: Planets*, 115(E3), 2010. doi: https://doi.org/10.1029/2009JE003456.

T. Guidat, S. Pochat, O. Bourgeois, and O. Souček. Landform assemblage in isidis planitia, mars: Evidence for a 3 ga old polythermal ice sheet. *Earth and Planetary Science Letters*, 411:253–267, 2015. ISSN 0012-821X. doi: https://doi.org/10.1016/j.epsl.2014.12.002.

H. Heinrich. Origin and consequences of cyclic ice rafting in the northeast atlantic ocean during the past 130,000 years. *Quaternary Research*, 29(2):142–152, 1988. ISSN 0033-5894. doi: https://doi.org/10.1016/0033-5894(88)90057-9.

R. C. A. Hindmarsh. A numerical comparison of approximations to the stokes equations used in ice sheet and glacier modeling. *Journal of Geophysical Research: Earth Surface*, 109(F1), 2004. doi: https://doi.org/10.1029/2003JF000065.

P. Holmlund and J. Fastook. A time dependent glaciological model of the weichselian ice sheet. *Quaternary International*, 27:53–58, 1995. ISSN 1040-6182. doi: https://doi.org/10.1016/1040-6182(94)00060-I.

R.LeB. Hooke. *Principles of Glacier Mechanics*. Cambridge University Press, 2 edition, 2005. doi: 10.1017/CBO9780511614231.

G. Hoppa, B.R. Tufts, R. Greenberg, and P. Geissler. Strike-slip faults on Europa: Global shear patterns driven by tidal stress. *Icarus*, 141(2):287–298, 1999. ISSN 00191035. doi: https://doi.org/10.1006/icar.1999.6185.

T.J. Hughes. Numerical reconstructions of paleo ice sheets. In G.H. Denton and T.J. Hughes, editors, *The Last Great Ice Sheets.*, pages 221–261. Wiley-Interscience, New York, 1981.

K. Hutter. *Theoretical Glaciology: Material Science of Ice and the Mechanics of Glaciers and Ice Sheets*. Mathematical Approaches to Geophysics 1. Springer Netherlands, 1983. ISBN 9789401511698; 9401511691; 9789401511674; 9401511675.

P. Huybrechts and T. Payne. The eismint benchmarks for testing ice-sheet models. *Annals of Glaciology*, 23:1–12, 1996. doi: 10.3189/S0260305500013197.

K. Kalousová. *Dynamics of icy satellites with a liquid phase*. PhD thesis, Charles University, 2014.

K. Kalousová, O. Souček, G. Tobie, and O. Choblet, G. Čadek. Water generation and transport below europa's strike-slip faults. *Journal of Geophysical Research: Planets*, 121(12):2444–2462, 2016. doi: https://doi.org/10.1002/2016JE005188.

W. M. Kaula. Tidal dissipation by solid friction and the resulting orbital evolution. *Rev. Geophys.*, 2(4):661–685, 1964. doi: 10.1029/RG002i004p00661.

M. Kihoulou, K. Kalousová, and O. Souček. Evolution of pluto's impact-deformed ice shell below sputnik planitia basin. *Journal of Geophysical Research: Planets*, 127(6):e2022JE007221, 2022. doi: https://doi.org/10.1029/2022JE007221.

S. D. King, Ch. Lee, P. E. Van Keken, W. Leng, S. Zhong, et al. A community benchmark for 2-D Cartesian compressible convection in the Earth's mantle. *Geophys. J. Int.*, 180(1):73–87, 01 2010. doi: 10.1111/j.1365-246X.2009.04413.x.

N. Kirchner, R. Greve, A.P. Stroeven, and J. Heyman. Paleoglaciological reconstructions for the tibetan plateau during the last glacial cycle: evaluating numerical ice sheet simulations driven by gcm-ensembles. *Quaternary Science Reviews*, 30(1): 248–267, 2011. ISSN 0277–3791. doi: https://doi.org/10.1016/j.quascirev.2010.11.006.

N. Kirchner, J. Ahlkrona, E.J. Gowan, P. Lötstedt, J.M. Lea, et al. Shallow ice approximation, second order shallow ice approximation, and full stokes models: A discussion of their roles in palaeo-ice sheet modelling and development. *Quaternary Science Reviews*, 135:103–114, 2016. ISSN 0277-3791. doi: https://doi.org/10.1016/j.quascirev.2016.01.013.

K. Kusahara, T. Sato, A. Oka, T. Obase, R. Greve, et al. Modelling the antarctic marine cryosphere at the last glacial maximum. *Annals of Glaciology*, 56(69): 425–435, 2015. doi: 10.3189/2015AoG69A792.

J. Kvorka, O. Čadek, G. Tobie, and G. Choblet. Does Titan's long-wavelength topography contain information about subsurface ocean dynamics? *Icarus*, 310: 149–164, August 2018. doi: 10.1016/j.icarus.2017.12.010.

A. König-Haagen, E. Franquet, E. Pernot, and D. Brüggemann. A comprehensive benchmark of fixed-grid methods for the modeling of melting. *International Journal of Thermal Sciences*, 118:69–103, 2017. ISSN 1290-0729. doi: https://doi.org/10.1016/j.ijthermalsci.2017.04.008.

J. Laskar, A.C.M. Correia, M. Gastineau, F. Joutel, B. Levrard, et al. Long term evolution and chaotic diffusion of the insolation quantities of mars. *Icarus*, 170 (2):343–364, 2004. ISSN 0019-1035. doi: https://doi.org/10.1016/j.icarus.2004.04.005.

L. Lliboutry. Permeability, brine content and temperature of temperate ice. *Journal of Glaciology*, 10(58):15–29, 1971. doi: 10.3189/S002214300001296X.

A. E. H. Love. *Lehrbuch der Elastizität*. B.G. Teubner Verlag, Leipzig, 1907.

D. R. MacAyeal. Large-scale ice flow over a viscous basal sediment: Theory and application to ice stream b, antarctica. *Journal of Geophysical Research: Solid Earth*, 94(B4):4071–4087, 1989. doi: https://doi.org/10.1029/JB094iB04p04071.

J.-B. Madeleine, F. Forget, J.W. Head, B. Levrard, F. Montmessin, et al. Amazonian northern mid-latitude glaciation on mars: A proposed climate scenario. *Icarus*, 203(2):390–405, 2009. ISSN 0019–1035. doi: https://doi.org/10.1016/j.icarus.2009.04.037.

H. M. Mader. The thermal behaviour of the water-vein system in polycrystalline ice. *Journal of Glaciology*, 38(130):359–374, 1992. doi: 10.3189/S0022143000002240.

Z. Martinec, C. Matyska, E. W. Grafarend, and P. Vaníček. Helmert's 2nd condensation method. *Manuscr. Geod.*, 18:417–421, 1993.

I. Matsuyama, M. Beuthe, H. C. F. C. Hay, F. Nimmo, and S. Kamata. Ocean tidal heating in icy satellites with solid shells. *Icarus*, 312:208–230, 2018. doi: 10.1016/j.icarus.2018.04.013.

Ch. McCarthy and J. C. Castillo-Rogez. *Planetary Ices Attenuation Properties*, pages 183–225. Springer New York, New York, NY, 2013. ISBN 978-1-4614-3076-6. doi: 10.1007/978-1-4614-3076-6.

D. McKenzie. The Generation and Compaction of Partially Molten Rock. *Journal of Petrology*, 25(3):713–765, 08 1984. ISSN 0022-3530. doi: 10.1093/petrology/25.3.713.

W. B. Moore and G. Schubert. The tidal response of europa. *Icarus*, 147(1):317–319, 2000. ISSN 0019-1035. doi: https://doi.org/10.1006/icar.2000.6460.

L. W. Morland. Unconfined ice-shelf flow. In C. J. Van der Veen and J. Oerlemans, editors, *Dynamics of the West Antarctic Ice Sheet*, pages 99–116, Dordrecht, 1987. Springer Netherlands. ISBN 978-94-009-3745-1.

L.W. Morland. Thermomechanical balances of ice sheet flows. *Geophysical & Astrophysical Fluid Dynamics*, 29(1-4):237–266, 1984. doi: 10.1080/03091928408248191.

F. Nimmo and E.s Gaidos. Strike-slip motion and double ridge formation on Europa. *Journal of Geophysical Research*, 107(E4):1–8, 2002. ISSN 0148-0227. doi: https://doi.org/10.1029/2000JE001476.

F. Nimmo and M. Manga. Geodynamics of Europa's Icy Shell. In Robert T. Pappalardo, William B. McKinnon, and Krishan K. Khurana, editors, *Europa*, page 381. 2009.

F. Nimmo, J. R. Spencer, R. T. Pappalardo, and M. E. Mullen. Shear heating as the origin of the plumes and heat flux on Enceladus. *Nature*, 447:289–291, May 2007. doi: 10.1038/nature05783.

J.F. Nye. The geometry of water veins and nodes in polycrystalline ice. *Journal of Glaciology*, 35(119):17–22, 1989. doi: 10.3189/002214389793701437.

F. Pattyn. A new three-dimensional higher-order thermomechanical ice sheet model: Basic sensitivity, ice stream development, and ice flow across subglacial lakes. *Journal of Geophysical Research: Solid Earth*, 108(B8), 2003. doi: https://doi.org/10.1029/2002JB002329.

F. Pattyn, L. Perichon, A. Aschwanden, B. Breuer, B. de Smedt, et al. Benchmark experiments for higher-order and full-stokes ice sheet models (ismip-hom). *The Cryosphere*, 2(2):95–108, 2008. doi: 10.5194/tc-2-95-2008.

F. Pattyn, C. Schoof, L. Perichon, R. C. A. Hindmarsh, E. Bueler, et al. Results of the marine ice sheet model intercomparison project, mismip. *The Cryosphere*, 6 (3):573–588, 2012. doi: 10.5194/tc-6-573-2012.

F. Pattyn, L. Perichon, G. Durand, L. Favier, O. Gagliardini, et al. Grounding-line migration in plan-view marine ice-sheet models: results of the ice2sea mismip3d intercomparison. *Journal of Glaciology*, 59(215):410–422, 2013. doi: 10.3189/2013JoG12J129.

V. F. Petrenko and R. W. Whitworth. *Physics of Ice*. Oxford University Press, 01 2002. ISBN 9780198518945. doi: 10.1093/acprof:oso/9780198518945.001.0001.

D. Pollard and R. M. DeConto. Description of a hybrid ice sheet-shelf model, and application to antarctica. *Geoscientific Model Development*, 5(5):1273–1295, 2012. doi: 10.5194/gmd-5-1273-2012.

C. Ritz. Time dependent boundary conditions for calculation of temperature fields in ice sheets. In *The Physical Basis of Ice Sheet Modelling*, volume 170 of *IAHS*, pages 207–216, 1987.

C. Ritz, A. Fabre, and A. Letréguilly. Sensitivity of a greenland ice sheet model to ice flow and ablation parameters: consequences for the evolution through the last climatic cycle. *Climate Dynamics*, 13:11–23, 1996. doi: https://doi.org/10.1007/s003820050149.

J.H. Roberts. The fluffy core of enceladus. *Icarus*, 258:54–66, 2015. ISSN 0019-1035. doi: https://doi.org/10.1016/j.icarus.2015.05.033.

M. Rovira-Navarro, M. Rieutord, T. Gerkema, L. R. M. Maas, W. der Wal, et al. Do tidally-generated inertial waves heat the subsurface oceans of Europa and Enceladus? *Icarus*, 321:126–140, 2019. doi: 10.1016/j.icarus.2018.11.010.

M. Rückamp, T. Kleiner, and A. Humbert. Comparison of ice dynamics using full-stokes and blatter–pattyn approximation: application to the northeast greenland ice stream. *The Cryosphere*, 16(5):1675–1696, 2022. doi: 10.5194/tc-16-1675-2022.

C.G. Salzmann. Advances in the experimental exploration of water's phase diagram. *The Journal of Chemical Physics*, 150(6):060901, 2019. doi: 10.1063/1.5085163.

H. Schmeling. *Partial Melting and Melt Segregation in a Convecting Mantle*, pages 141–178. Springer Netherlands, Dordrecht, 2000.

B. E. Schmidt, D. D. Blankenship, G. W. Patterson, and P. M. Schenk. Active formation of 'chaos terrain' over shallow subsurface water on europa. *Nature*, 479: 502–505, 2011. doi: 10.1038/nature10608.

E. M. Schulson and P. Duval. *Creep and Fracture of Ice*. Cambridge University Press, 2009. doi: 10.1017/CBO9780511581397.

D. R. Scott and D. J. Stevenson. Magma solitons. *Geophysical Research Letters*, 11 (11):1161–1164, 1984. doi: https://doi.org/10.1029/GL011i011p01161.

D. R. Scott and D. J. Stevenson. A self-consistent model of melting, magma migration and buoyancy-driven circulation beneath mid-ocean ridges. *Journal of Geophysical Research: Solid Earth*, 94(B3):2973–2988, 1989. doi: https://doi.org/10.1029/JB094iB03p02973.

H. Seddik, R. Greve, T. Zwinger, F. Gillet-Chaulet, and O. Gagliardini. Simulations of the greenland ice sheet 100 years into the future with the full stokes model elmer/ice. *Journal of Glaciology*, 58(209):427–440, 2012. doi: 10.3189/2012JoG11J177.

K. M. Soderlund, B. E. Schmidt, J. Wicht, and D. D. Blankenship. Ocean-driven heating of Europa's icy shell at low latitudes. *Nat. Geosci.*, 7:16–19, January 2014. doi: 10.1038/ngeo2021.

C. Sotin, J.W. Head, and G. Tobie. Tidal heating of upwelling thermal plumes and the origin of lenticulae and chaos melting. *Geophys. Res. Let.*, 29:1233, doi:10.1029/2001GL013844, 2002.

O. Souček and Z. Martinec. Iterative improvement of the shallow-ice approximation. *Journal of Glaciology*, 54(188):812–822, 2008. doi: 10.3189/002214308787779924.

O. Souček and Z. Martinec. Ismip-heino experiment revisited: effect of higher-order approximation and sensitivity study. *Journal of Glaciology*, 57(206):1158–1170, 2011. doi: 10.3189/002214311798843278.

O. Souček, O. Bourgeois, P. Stéphane, and T. Guidat. A 3 ga old polythermal ice sheet in isidis planitia, mars: Dynamics and thermal regime inferred from numerical modeling. *Earth and Planetary Science Letters*, 426:176–190, 2015. ISSN 0012-821X. doi: https://doi.org/10.1016/j.epsl.2015.06.038.

O. Souček, M. Běhounková, O. Čadek, J. Hron, G. Tobie, et al. Tidal dissipation in Enceladus' uneven, fractured ice shell. *Icarus*, 328:218–231, 2019. ISSN 0019-1035. doi: 10.1016/j.icarus.2019.02.012.

M. Spiegelman. Flow in deformable porous media. part 1 simple analysis. *Journal of Fluid Mechanics*, 247:17–38, 1993. doi: 10.1017/S0022112093000369.

M. Spiegelman and D. McKenzie. Simple 2-d models for melt extraction at mid-ocean ridges and island arcs. *Earth and Planetary Science Letters*, 83(1):137–152, 1987. ISSN 0012-821X. doi: https://doi.org/10.1016/0012-821X(87)90057-4.

O. Šrámek, Y. Ricard, and D. Bercovici. Simultaneous melting and compaction in deformable two-phase media. *Geophysical Journal International*, 168(3):964–982, 03 2007. ISSN 0956-540X. doi: 10.1111/j.1365-246X.2006.03269.x.

L. Tarasov and R.W. Peltier. Greenland glacial history and local geodynamic consequences. *Geophysical Journal International*, 150(1):198–229, 07 2002. ISSN 0956-540X. doi: 10.1046/j.1365-246X.2002.01702.x.

L Tarasov, A.S. Dyke, M.R. Neal, and W.R. Peltier. A data-calibrated distribution of deglacial chronologies for the north american ice complex from glaciological modeling. *Earth and Planetary Science Letters*, 315-316:30–40, 2012. ISSN 0012-821X. doi: https://doi.org/10.1016/j.epsl.2011.09.010. Sea Level and Ice Sheet Evolution: A PALSEA Special Edition.

G. Tobie, G. Choblet, and C. Sotin. Tidally heated convection: Constraints on Europa's ice shell thickness. *J. Geophys. Res. Planets*, 108(E11):5124, 2003. doi: 10.1029/2003JE002099.

G Tobie, A Mocquet, and C Sotin. Tidal dissipation within large icy satellites: Applications to Europa and Titan. *Icarus*, 177(2):534–549, 2005. doi: 10.1016/j.icarus.2005.04.006.

G. Tobie, O. Čadek, and C. Sotin. Solid tidal friction above a liquid water reservoir as the origin of the South Pole Hotspot on Enceladus. *Icarus*, 196(2):642–652, 2008. doi: 10.1016/j.icarus.2008.03.008.

Robert Tyler. Comparative estimates of the heat generated by ocean tides on icy satellites in the outer solar system. *Icarus*, 243:358–385, 2014. ISSN 0019-1035. doi: https://doi.org/10.1016/j.icarus.2014.08.037.

C.J. van der Veen. Fracture mechanics approach to penetration of surface crevasses on glaciers. *Cold Regions Science and Technology*, 27(1):31–47, 1998. ISSN 0165-232X. doi: https://doi.org/10.1016/S0165-232X(97)00022-0.

S. Webb and I. Jackson. Anelasticity and microcreep in polycrystalline mgo at high temperature: an exploratory study. *Phys Chem Minerals*, 30(I):157–166, 2003. doi: 10.1007/s00269-003-0299-1.

J. Weertman. On the sliding of glaciers. *Journal of Glaciology*, 3(21):33–38, 1957. doi: 10.3189/S0022143000024709.

Collection of publications P

Author's contribution to the publications

All the publications appended in this thesis are works that I have significantly contributed to. In particular, I have participated in discussions, interpretation of the results and writing the manuscripts in all the papers. I have solely developed the computational methodology and its numerical implementation and I also performed all the numerical simulations in [P1] and [P2]. In [P3], [P4], and [P5], I was substantially involved in the code development, as well as in performing the numerical simulations. In [P8], [P9] and [P10], I contributed to a large extent to the theoretical model development and to its numerical implementation. Finally, [P7], [P6] and [P11] are three manuscripts that I have co-written with my Ph.D. students and where I participated on the development and numerical implementation of the models.

List of appended publications

P1 Souček, O., Martinec, Z. (2011). ISMIP-HEINO experiment revisited: Effect of higher-order approximation and sensitivity study, J. Glaciol., 57(206), 1158–1170.

P2 Souček, O., Bourgeois, O., Pochat, S., Guidat, T. (2015). A 3 Ga old polythermal ice sheet in Isidis Planitia, Mars: dynamics and thermal regime inferred from numerical modeling, Earth Planet. Sci. Lett., 426, 176–190.

P3 Souček, O., Hron, J., Běhounková, M., Čadek, O. (2016). Effect of the tiger stripes on the deformation of Saturn's moon Enceladus, Geophys. Res. Lett., 43(14), 7417–7423.

P4 Běhounková, M., Souček, O., Hron, J., Čadek, O. (2017). Plume activity and tidal deformation of Enceladus influenced by faults and variable ice shell thickness, Astrobiology, 17(9), 941–954.

P5 Souček, O., Běhounková, M., Čadek, O., Hron, J., Tobie, G., Choblet, G. (2019). Tidal dissipation in Enceladus' uneven, fractured ice shell, Icarus, 328, 218–231.

P6 Pleiner Sládková, K., Souček., O., Běhounková M. (2021). Enceladus' tiger stripes as frictional faults: Effect on stress and heat production, Geophys. Res. Lett, 48(19), 1–9.

P7 Sládková, K., Souček., O., Kalousová, K., Běhounková, M. (2020). Tidal walking on Europa's strike-slip faults - insight from numerical modeling, J. Geophys. Res. - Planets, 125, 1–24.

P8 Souček, O., K. Kalousová, Čadek, O. (2014). Water transport in planetary ice shells by two-phase flow - a parametric study, Geophys. Astro. Fluid, 108(6), 639–666.

P9 Kalousová, K., Souček, O., Tobie, G., Choblet, G., Čadek, O. (2014). Ice melting and downward transport of meltwater by two-phase flow in Europa's ice shell, J. Geophys. Res. - Planets, 119(3), 532–549.

P10 Kalousová, K., Souček, O., Tobie, G., Choblet, G., Čadek, O. (2016). Water generation and transport below Europa's strike-slip faults, J. Geophys. Res. - Planets, 121(12), 2444–2462.

P11 Malík, J., Souček, O. (2022). Semi-analytical benchmark for the Stefan problem in arbitrary dimension - assessing accuracy of enthalpy-based methods, Int. J. Numer. Methods Heat Fluid Flow, *ahead of print*, https://doi.org/10.1108/HFF-09-2021-0647.

P1

ISMIP-HEINO experiment revisited: Effect of higher-order approximation and sensitivity study

Souček, O., Martinec, Z.

Published in *Journal of Glaciology 57(206)*, 1158–1170 (2011)

doi: https://doi.org/doi:10.3189/002214311798843278

P2

A 3 Ga old polythermal ice sheet in Isidis Planitia, Mars: dynamics and thermal regime inferred from numerical modeling

Souček, O., Bourgeois, O., Pochat, S., Guidat, T.

Published in *Earth and Planetary Science Letters 426*, 176–190 (2015)

doi: https://doi.org/doi:10.1016/j.epsl.2015.06.038.

P3

Effect of the tiger stripes on the deformation of Saturn's moon Enceladus

Souček, O., Hron, J., Běhounková, M., Čadek, O.

Published in *Geophysical Research Letters 43(14)*, 7417–7423 (2016)

doi: https://doi.org/10.1002/2016GL069415.

P4

Plume activity and tidal deformation of Enceladus influenced by faults and variable ice shell thickness

Běhounková, M., Souček, O., Hron, J., Čadek, O.

Published in *Astrobiology 17(9)*, 941–954 (2017)

doi: https://doi.org/10.1089/ast.2016.1629.

P5

Tidal dissipation in Enceladus' uneven, fractured ice shell

Souček, O., Běhounková, M., Čadek, O., Hron, J., Tobie, G., Choblet, G.

Published in *Icarus 328*, 218–231 (2019)

doi: https://doi.org/10.1016/j.icarus.2019.02.012.

P6

Enceladus' tiger stripes as frictional faults: Effect on stress and heat production

Pleiner Sládková, K., Souček., O., Běhounková M.

Published in *Geophysical Research Letters 48(19)*, 1–9 (2021)

doi: http://doi.org/10.1029/2021GL094849.

P7

Tidal walking on Europa's strike-slip faults – insight from numerical modeling

Sládková, K., Souček., O., Kalousová, K., Běhounková, M.

Published in *Journal of Geophysical Research - Planets 125*, 1–24 (2020)

doi: https://doi.org/10.1029/2019JE006327.

P8

Water transport in planetary ice shells by two-phase flow – a parametric study

Souček, O., K. Kalousová, Čadek, O.

Published in *Geophysical and Astrophysical Fluid Dynamics 108(6)*, 639–666 (2014)

doi: https://doi.org/10.1080/03091929.2014.969251.

P9

Ice melting and downward transport of meltwater by two-phase flow in Europa's ice shell

Kalousová, K., Souček, O., Tobie, G., Choblet, G., Čadek, O.

Published in *Journal of Geophysical Research - Planets 119(3)*, 532–549 (2014)

doi: https://doi.org/10.1002/2013JE004563.

P10

Water generation and transport below Europa's strike-slip faults

Kalousová, K., Souček, O., Tobie, G., Choblet, G., Čadek, O.

Published in *Journal of Geophysical Research - Planets 121(12)*, 2444–2462 (2016)

doi: http://dx.doi.org/10.1002/2016JE005188.

P11

Semi-analytical benchmark for the Stefan problem in arbitrary dimension - assessing accuracy of enthalpy-based methods

Malík, J., Souček, O.

Published in *International Journal of Numerical Methods for Heat & Fluid Flow, ahead-of-print*, (2022)

doi: https://doi.org/10.1108/HFF-09-2021-0647.